EZH2 INHIBITOR GSK126 FOR CANCER TREATMENT: METABOLISM, DRUG TRANSPORTER AND RAT PHARMACOKINETIC STUDIES

Amit Kumar[a]; Vijay Kumar[a]; Janet W. Lightner[b]; Anaheed L. Little[a]; Promsuk Jutabha[c]; Hitoshi Endou[d]; Peter J. Rice[a,b]; Philip Reigan[a]; Rajeev Vibhakar[e]; Peter Harris[e]; Ilango Balakrishnan Ilango[e]; Sujatha Venkataraman[e]; Marielle Nebout[f]; Jean-Francois Peyron[f]; and Michael F. Wempe[a,g,]*

[a]Department of Pharmaceutical Sciences, School of Pharmacy, University of Colorado Denver Anschutz Medical Campus, Aurora, CO 80045, USA

[b]Department of Pharmacology, East Tennessee State University Johnson City, TN 37614, USA

[c] Dokkyo Medical University School of Medicine, Tochigi, Japan

[d]Department of Pharmacology and Toxicology, Kyorin University School of Medicine, Mitaka, Tokyo, 181-8611 Japan

[e] Department of Pediatrics, School of Medicine, University of Colorado Denver, Anschutz Medical Campus, Aurora, CO 80045, USA

[f]INSERM, U1065, Centre Méditerranéen de Médecine Moléculaire (C3M), Equipe Inflammation, Cancer, Cellules Souches Cancéreuses, Nice, France.

[g]University of Colorado Cancer Center, University of Colorado Denver, Aurora, Colorado 80045, USA

Email addresses, co-authors: Amit Kumar – amit.2.kumar@ucdenver.edu; Vijay Kumar – vijay.kumar@ucdenver.edu; Janet W. Lightner – lightner@mail.etsu.edu; Anaheed L. Little – anaheed.little@colorado.edu; Promsuk Jutabha – pjutabha@hotmail.com; Hitoshi Endou – endouh@ks.kyorin-u.ac.jp; Peter J. Rice – peter.rice@ucdenver.edu; Philip Reigan – philip.reigan@ucdenver.edu; Rajeev Vibhakar – rajeev.vibhakar@ucdenver.edu; Peter Harris – peter.harris@ucdenver.edu; Ilango Balakrishnan Ilango – ilango.balakrishnan@ucdenver.edu; Sujatha Venkataraman – sujatha.venkataraman@ucdenver.edu; Marielle Nebout – marielle.nebout@unice.fr; Jean-Francois Peyron – jean-francois.peyron@unice.fr

Keywords—EZH2 Inhibitor; GSK126 and GSK126-d7; OAT's; Drug Metabolism; Rat Pharmacokinetic Study

* Corresponding author. Tel.: 303-724-8982; fax: 303-724-6148; e-mail: michael.wempe@ucdenver.edu

Abstract—Histone lysine methyl transferase 2 (EZH2) inhibitor GSK126 and a novel deuterated internal standard GSK126-d_7 were chemically prepared. We performed *in vitro* experiments using the prepared GSK126 to: i) confirm *in vitro* EZH2 inhibitory activity; ii) conduct Sprague-Dawley (SD) rat liver microsomal incubations and identified Phase I metabolites; iii) determine whether or not GSK126 was an Organic Anion Transporter (OAT) substrate; and, iv) determine oral bioavailability by conducting oral and orbital sinus dosing (OSD) experiments and determining blood concentration versus time profiles. GSK126 was shown to decrease the expression of H3K27Me3 protein in medulloblastoma D283 cells and was able to decrease cell viability in KO99L cells, a novel T cell lymphoma cell line. Three *in vitro* hepatic Phase I mono-oxidative metabolites (**L-M1**, **L-M2** and **L-M3**) were observed and also detected in rat liver and urine samples from the *in vivo* studies. GSK126 was found to be an OAT1 and OAT2 substrate, but not an OAT3 or OAT4 substrate. Our Pharmacokinetic (PK) results indicate: 1) GSK126 has very poor oral bioavailability (< 2%); 2) co-administration of probenecid, a prototypical OAT inhibitor, did not significantly alter observed PK; and 3) tissue distribution studies demonstrate that GSK126 predominately distributes to the liver and kidneys after an OSD.

1. Introduction

In the United States, cancer death (*e.g.* prostate, breast, lung, colon, melanoma, bladder, non-Hodgkin lymphoma, kidney, thyroid and endometrial) estimates for 2014 approached nearly six hundred thousand humans (http://seer.cancer.gov/statfacts/html/all.html) . Cancer tissues/cells are well known to exhibit accelerated growth rate. In general, compared to normal cells, cancer cells have altered metabolism; for example, cancer cells are known to possess enhanced glucose metabolism (Warburg, 1956). It is now established that primary human tumors and tumor cell lines also highly express L-amino acid transporter 1 (hLAT1) (Yanagida et al., 2001). Normal cells – except in specific organs (e.g. eye) – express hLAT2 whereas cancer cells predominately express hLAT1. Thus, tumors and tumor cell lines not only have altered metabolism, but they also have altered transporter protein profiles as well. Another interesting discovery regarding how cancer cells mediate growth involves histone lysine methyl-transferase 2 (EZH2). EZH2, also referred to as 'Enhancer of Zeste Homologue 2', plays a role in tumorigenesis (Varambally et al., 2002; Kleer et al., 2003; Varambally et al., 2008; Wagener et al., 2010; Takawa et al., 2011). A catalytic subunit of the Polycomb Repressive Complex 2 (PRC2) (Cardoso et al., 2000), EZH2 catalyzes trimethylation of lysine 27 residue of histone H3 (H3K27me3) via methyl group transfer on cofactor *S*-(adenosyl)-*L*-methionine (SAM). Histone H3, one of the five main histone proteins, is a chromatin structural component found in eukaryotic cells (Bhasin et al., 2006). Increasing the levels of H3K27me3 may contribute to the aggressiveness of cancer in various tumors like brain (Smits et al., 2010), breast (Zeidler et al., 2006; Kleer, 2009), kidney (Wagener et al., 2008), lung (Crea et al., 2011), lymphoma (Be´guelin et al., 2013; Yan et al., 2013), and prostate (Takawa et al., 2011). As EZH2 inhibition may lead to transcriptional repression of the affected target gene, the development of potent EZH2 inhibitors has become an attractive therapeutic strategy.

As summarized in **Figure 1**, various EZH2 inhibitors have been described in the literature and include 3-deazaneplanocin A (DZNep) **1**, El1 **2**, EPZ005687 **3**, GSK126 **4**, GSK343 **5**, GSK926 **6** and UNC1999 **7**. DZNep was initially reported to selectively inhibit methylation of lysine 27 on histone H3 (H3K27me3) and lysine 20 on histone H4 (H4K20me3) as well as induce cancer cell apoptosis (Tan et al., 2007); however, DZNep **1** has been shown to globally inhibit both repressive and active histone methylation (Miranda et al., 2009) and reported to be a PRC2 inhibitor against prostate cancer cells (Crea et al., 2011). Another potential small molecule inhibitor named El1 **2** was developed by Qi *et al.* (Qi et al., 2012); **2** inhibits EZH2 activity through competition with the cofactor SAM and selective against EZH2 over homolog EZH1. By conducting *in vitro* studies, Knutson *et al.* (Knutson et al., 2012) discovered EPZ005687 **3**, a selective and potent inhibitor of wild-type and mutant EZH2-containing PRC2 activity (*Ki* of 24 nM). In addition, McCabe *et al*. (McCabe et al., 2012) extensively prepared and investigated a small molecule library. The library was screened for inhibitory activity to illustrate GSK126 **4** as a potent (low nM) EZH2 inhibitor. GSK126 **4** inhibits both wild-type and mutant EZH2, a histone-lysine methyltransferase with similar potency; **4** has a high degree of EZH2 selectivity, including EZH1 which has 96% consistency to EZH2 within its set domain and 76% overall sequence similarity. Verma

et al. (Verma et al., 2012) have also studied GSK343 **5** and GSK926 **6**, which are analogs in the same chemical series as **4**. Lastly, Konze *et al.* (Konze et al., 2013) described the first orally bioavailable inhibitor, UNC1999 **7**. Analog **7** has high *in vitro* potency for the wild-type and mutant EZH2 as well as EZH1, and highly selective for EZH2 and EZH1 over a broad range of epigenetic and non-epigenetic targets; **7** was designed to be competitive with the cofactor SAM and non-competitive with the peptide substrate.

Figure 1. EZH2 inhibitor examples

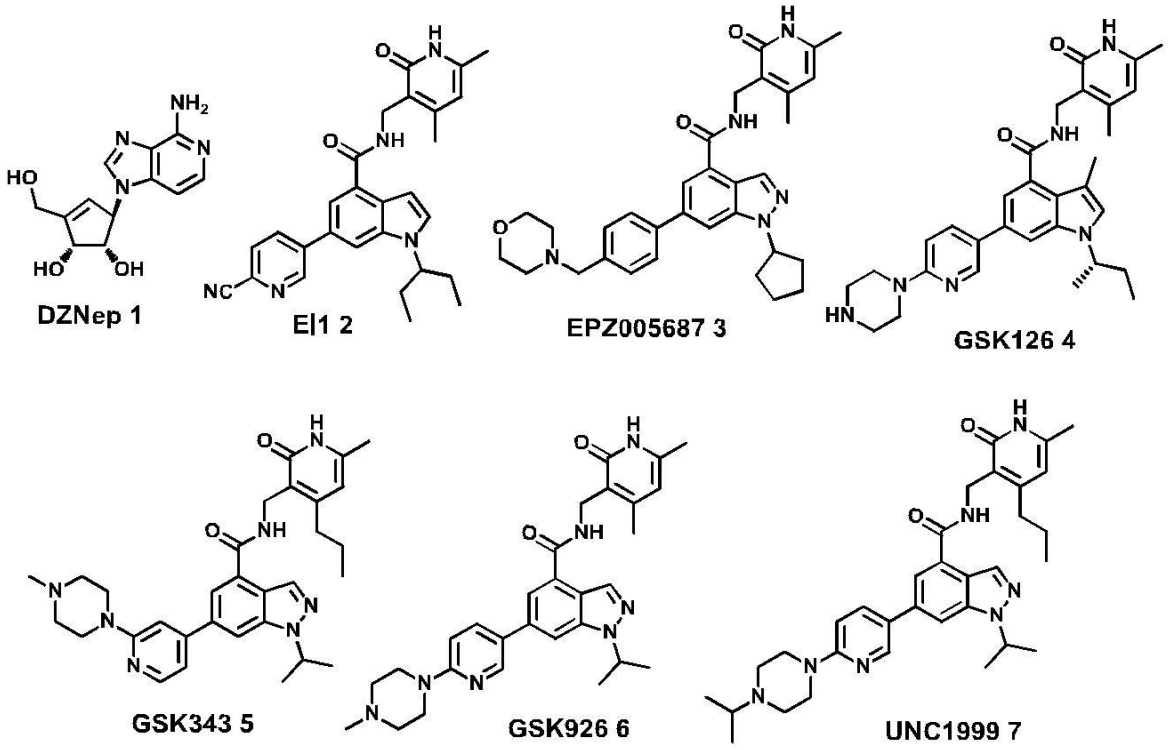

In our ongoing efforts to assess potential synergistic and/or additive effects on cancer cell survival by exploiting various cancer therapeutic agents (Rosilio et al. 2015), we desired to investigate the utility of an EZH2 inhibitor; consequently, we selected GSK126 **4**. It has been established that **4** can inhibit the *in vivo* growth of EZH2 mutant DLBCL (diffuse large B-cell lymphoma) in a dose dependent manner via a rodent (mouse) xenograft model (McCabe et al. 2012). In the current study, we performed chemical synthesis to afford the desired drug and prepared a novel deuterated analog which was subsequently used as an LC/MS-MS analytical internal standard (IS). A liquid chromatography/mass spectrometry-mass spectrometry (LC/MS-MS) method was developed and used to quantitate **4** from biological samples (*i.e.* cells, blood, organs). We utilized *in vitro* methods (rat liver microsomes and cell lines expressing drug transporters) and also performed *in vivo* experiments in male Sprague-Dawley (SD) rats to produce experimental observations regarding the absorption, distribution, metabolism, and excretion (ADME) of **4**.

2. Results and Discussions

The selective EZH2 inhibitor known as GSK126 **4** has recently become commercially available from a few vendors; for example, it may be procured from Cayman Chemical Company (Ann Arbor, Michigan). However, our research needs and financial constraints extended to multiple research groups; it required multi-gram quantities of the drug substance and it was thus more economical to prepare **4** ourselves than to merely procure it. As there are some scientific publications which provide various synthetic procedural information to prepare molecules such as **2**-**7** (Brackley et al., 2011; Knutson et al., 2012; McCabe et al., 2012; Qia et al., 2012; Verma et al., 2012; Konze et al., 2013), we prepared **4** (**Scheme 1**) by brominating 2-methyl-3-nitro benzoic acid to give bromo-nitro-benzoic acid **8**. Compound **8** was then subjected to addition & cyclization reactions to yield bromo-indole methyl ester **9**. Prepared from the commercially available chiral alcohol, selective stereochemistry was incorporated using two sequential SN2 reactions; first producing chiral alkyl halide **10** and then coupled to **9** to give the desired (*S*)-enantiomer **11**. Incorporating the 3-methyl functionality into the indole ring required two chemical steps; first, the formyl group (-CHO) was added to the indole to give **12** which was fully reduced to furnish methyl ester **13**. Methyl ester **13** was hydrolyzed under basic conditions to produce chiral carboxylic acid **14**. From a strategic point of view, the incorporation of selective chirality early into the synthetic scheme equated to a more expensive chemical synthesis. Consequently, in an attempt to increase overall yield and decrease our costs, we sought to delay the incorporation of the chiral sec-butyl functionality. We first added the formyl group into **9** to produce **15** which was then reduced to

Scheme 1. Synthesis of GSK126, Compound **4**

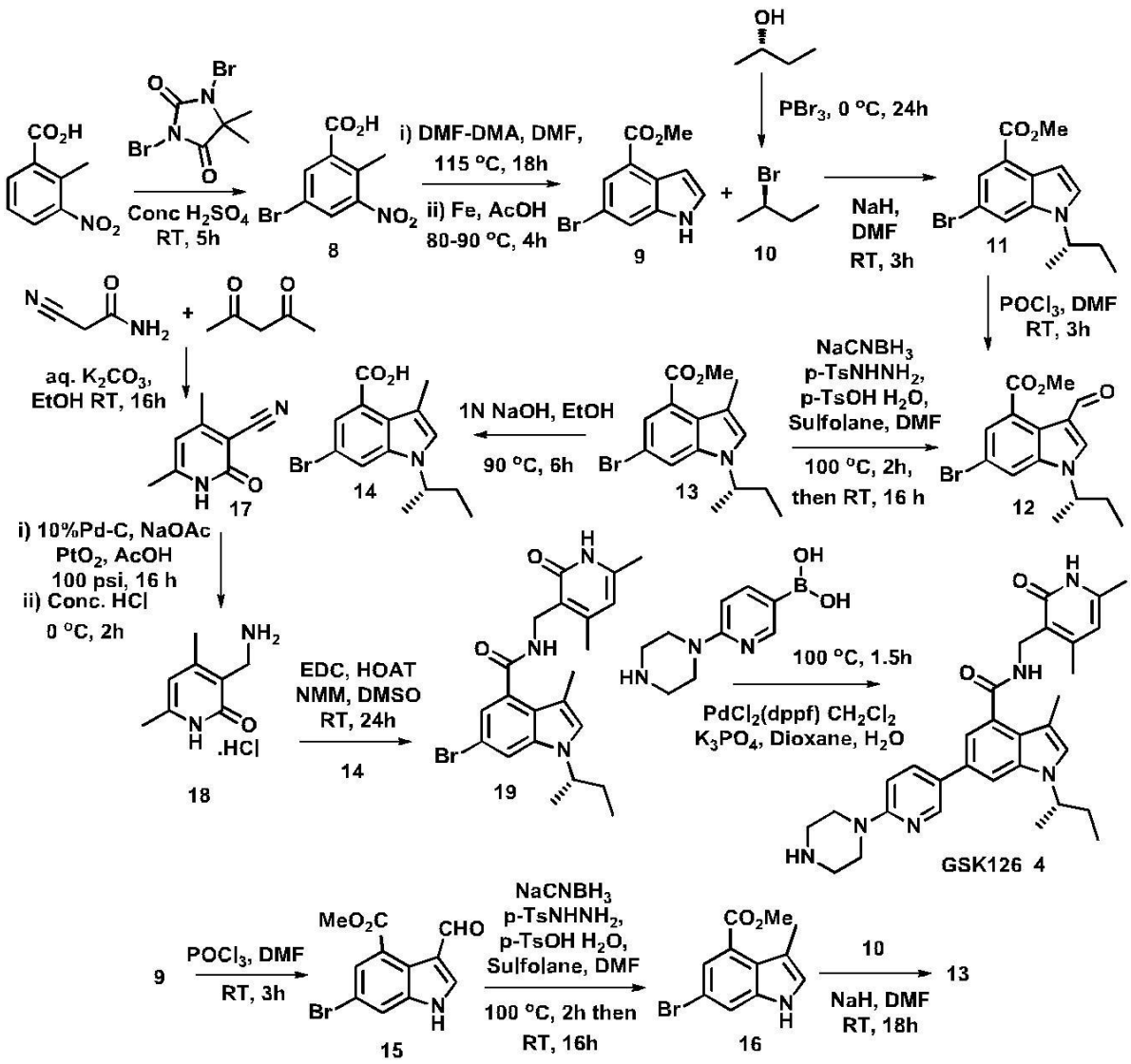

3-methyl-indole **16**; thereafter, the chirality was then incorporated to afford **13**. While the reaction conditions are not optimized, these results clearly illustrate that on a per gram scale production comparison of **13**, the second route required one-third less chiral reagent. Hence, this provides some improvement to the overall synthetic preparation of compound **4**. Next, cyano-acetamide condensation with acetyl acetone under basic conditions produced carbonitrile **17** which was catalytically reduced to afford amine **18** and isolated as the hydrochloride salt. The chiral sec-butyl indole acid **14** and amine **18** were then coupled to generate amide **19**. Lastly, amide **19** was coupled with boronic acid 1-(5-(4,4,5,5-tetramethyl-1,3,2-dioxaborolan-2-yl)pyridin-2 yl)piperazine to produce the desired EZH2 inhibitor **4**. Furthermore, our primary research goal was to successfully prepare drug substance and then to generate pharmacokinetic (PK) and tissue distribution (PD, pharmaco-dynamic) data to be used to guide dosing regimen for future tumor animal models experiments; consequently,

we conducted various experiments in a normal (healthy) rat model. As sound analytics dictate the incorporation of an internal standard (IS), we sought to prepare a novel deuterated GSK126 analog. As presented in synthetic **Scheme 2**, we prepared a deuterated analog by complete hydrogen/deuterium exchange within acetyl acetone to produce acetyl acetone-d8 **20**, which was reacted with cyano-acetamide under deuterated basic conditions to afford cyano-d8 **21**. Following similar conditions to prepare amine **18**, deuterated amine **22** – which now contains seven deuterated atoms due to deuterium/proton exchange – was obtained from **21** via reduction and then coupled with **14** to afford deuterated amide **23**. Deuterated **23** was then attached with 1-(5-(4,4,5,5-tetramethyl-1,3,2-dioxaborolan-2-yl)pyridin-2-yl)piperazine to produce GSK126-d7 **24**. To our knowledge, the deuterated analog **24** is novel and not previously reported.

Scheme 2. Synthesis of GSK126-d7, Compound **24**

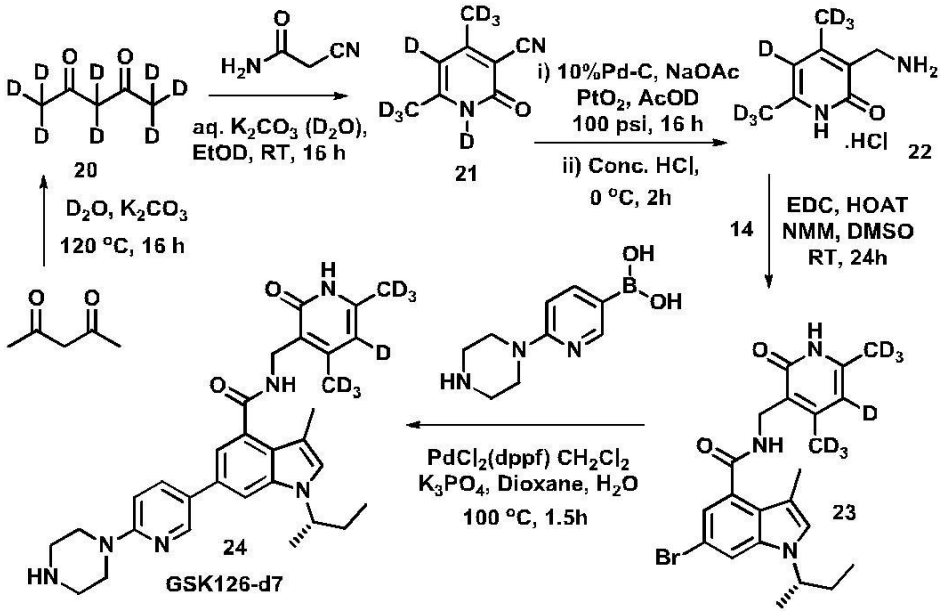

Upon the successful preparation of **4**, it was imperative to demonstrate *in vitro* biological activity. Consequently, we utilized two different cell lines. The first was D283, a medullo-blastoma cell line. We incubated cells in the absence or presence of GSK126 **4** to demonstrate a dose and time dependency on D283 cell viability, **Figure 2A**. For example, on days 6 & 8, compared to control (no **4**), GSK126 displayed a statistically significant cell viability decrease trend ($P < 0.001$) at 2.0 and 6.0 □M, respectively; the 0.5 □M dose of **4** was not statistically different than control. In addition, as depicted in **Figure 2B**, drug treated cells displayed a significant and concentration dependent decrease in H3K27me3 protein level. These data illustrate that our synthetically prepared **4** displayed the anticipated *in vitro* biological activity by decreasing the expression of H3K27Me3 protein.

Figure 2A. D283 cell viability (n = 4-5 ± SD) as a function of GSK126 concentration and time; ● = DMSO control, no GSK126; ■ = 0.5 μM GSK126; ▲ = 2.0 μM GSK126; and, ▼ = 6.0 μM; *** = P < 0.001. GSK126.

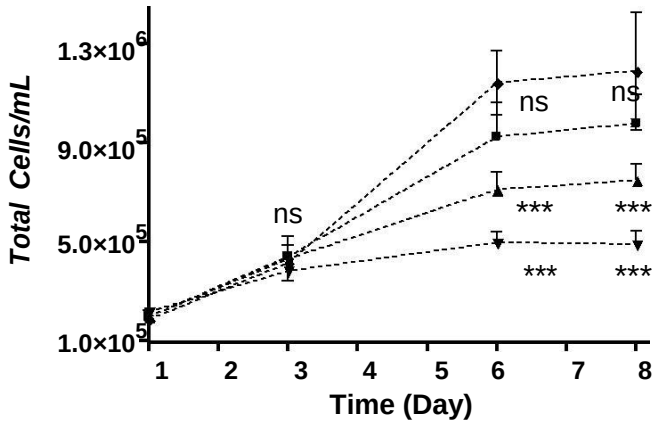

Figure 2B. D283 cells dosed with GSK126 and Western blot analysis. Top row displays H3K27me3 protein expression, bottom row is H3 loading control.

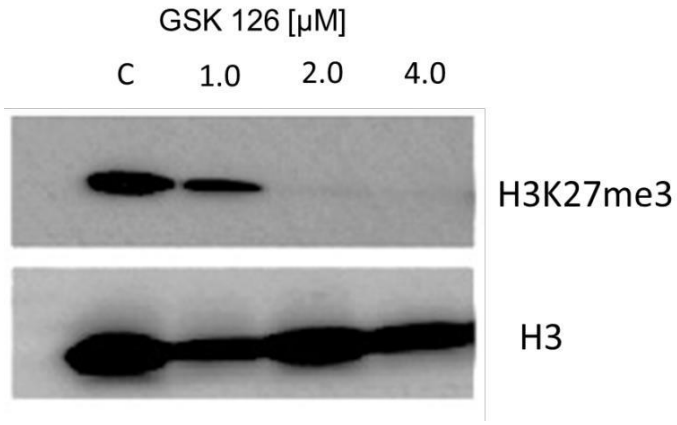

As another example, we also utilized KO99L cells as an in vitro leukemia model. KO99L is a new cell line derived from a T cell lymphoma (tPTEN-/-) mouse model generated after the T-lymphocyte specific inactivation of the *PTEN* tumor suppressor gene (Rosilio et al. 2015). The KO99L cells possess elevated LAT1 (Rosilio et al., 2015). From our experience, cancer cell lines with elevated LAT1 expression appear more resistant to therapeutic treatment compared to their lower LAT1 expressing cells (Rosilio et al., 2015). Consequently, KO99L cell viability was

Figure 3. A: tPTEN-/- K099L cell line and GSK126 concentration dependent cell viability; n = 3 ± SD, * = P < 0.01. **B:** tPTEN-/- K099L cell line and GSK126 concentration dependent cell metabolism; n = 3 ± SD, * = P < 0.01.

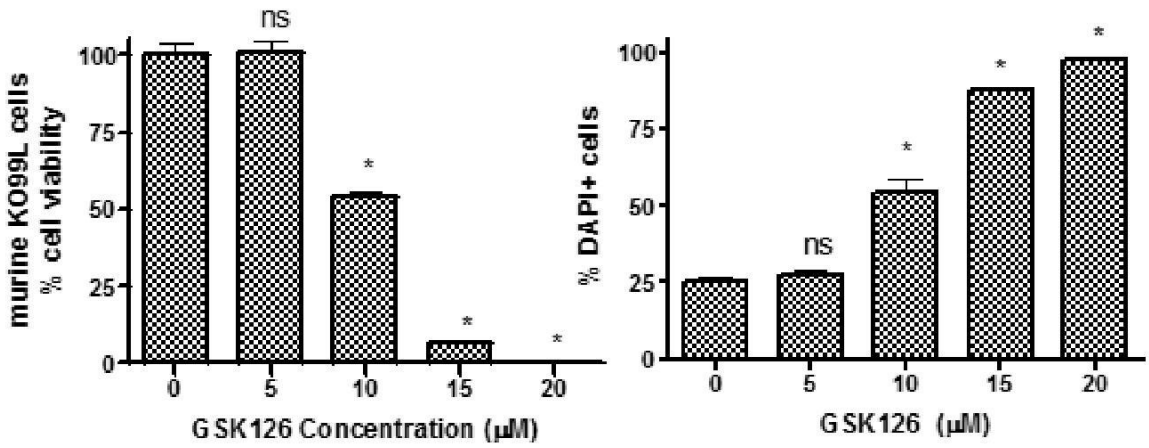

compared in the absence and presence of various concentrations of GSK126 **4**. As summarized in **Figure 3A** and **Figure 3B**, cell viability was assessed by monitoring mitochondrial dehydrogenase activity and cell death (DAPI staining), respectively. The average half maximal effective concentrations (EC50) were 10 □M and 11 □M for **Figure 3A** and **3B**, respectively. From these data, **4** required higher drug concentrations to achieve *in vitro* biological activity in this T cell lymphoma mouse cell model. We presume that the observed in vitro activity was a function of the established EZH2 inhibitory properties but that these cells with higher LAT1 expression have additional mechanisms (i.e. higher essential amino acid sequestering potential) to combat chemical attacks. This is a main rationale for why multiple therapy approaches, in our opinion, are needed and will be far more advantageous compared to single drug target therapy approaches. These results help to set the stage for our future on-going in vivo co-therapy approach experiments.

Prior to performing the *in vivo* PK experiments, we also probed Phase I *in vitro* metabolism of **4** using SD liver microsomes in the presence of co-factor NADPH; the cofactor required for CYP catalyzed biotransformation. As presented in **Figure 4**, we observed three liver *in vitro* biotransformation metabolites (M + 16 amu) denoted as **L-M1**, **L-M2** and **L-M3**. In accordance with the MS/MS daughter fragmentation patterns, metabolites **L-M1** and **L-M3** displayed oxidation in the lower region of the molecule (*i.e.* A = (*S*)-1-sec-butyl-3-methyl-6-(6-(piperazin-1-yl)pyridin-3-yl)-1H-indole-4-carboxamide portion; 543.3 □ 391.3 *m/z*), whereas metabolite **L-M2** was oxidized on the 4,6-dimethyl-2-oxo-1,2-dihydropyridin-3-yl)methyl functionality (upper region of molecule, B; 543.4 □ 375.2 *m/z*). The metabolite denoted as **L-M2** had a similar daughter ion as parent drug GSK126 **4** 527.4 □ 375.2 *m/z* (see supplementary materials section). The LC/MS-MS standard curves were prepared from nine standard curve concentrations (n = 4) representing concentrations between 0.8 – 1314 ng/mL. A standard curve was prepared for each:

Figure 4. Representative LC/MS-MS chromatogram of rat liver microsomal (2.0 mg/mL) incubation in the presence of GSK126 (10 μM) and NADPH (1.0 mM).

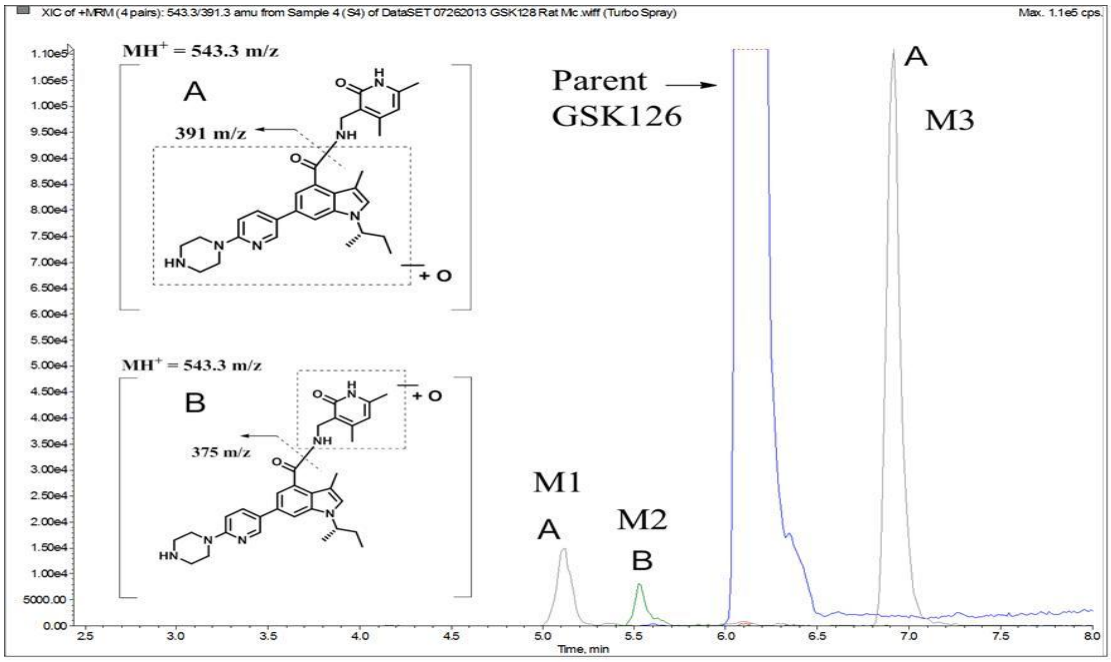

brain, blood, kidney, liver and urine. The limit of detection (LOD) values were ≤ 0.5 ng/mL (ng/g tissue) while the limit of quantitation (LOQ) were approximately 1.5 ng/mL (blood) and 1.5 ng/g (tissue homogenates). All standard curve data were fitted to a $1/x^2$ weighted linear regression; brain, blood, kidney, liver and urine standard curves had correlation coefficients (R^2) of 0.9989, 0.9999, 0.9999, 0.9993, and 0.9989, respectively.

Having a general research interest to further investigate the interplay of drug transporters on Pharmacokinetics (PK) (Anzai et al., 2011), we probed whether or not **4** was a substrate of organic anion transporters (OAT). Renal proximal tubular cells possess various transporter proteins which help to maintain physiological homeostasis (Chiba et al., 2013). Numerous organic compounds (*e.g.* endogenous compounds, drugs, toxins, etc.) are secreted into proximal tubular cells from the blood across the basolateral membrane followed by extrusion across the brush-border membrane into tubular fluid (Pritchard et al., 1993). We probed the *in vitro* uptake of **4** in S2-cells (mock and OAT expressing); these data (**Figure 5**) suggest that EHZ2 inhibitor **4** is an hOAT1 and hOAT2 substrate, but not an hOAT3 or hOAT4 substrate. The ramification of **4** being an OAT1 substrate equated to a potential *in vivo* Drug-Drug Interaction (DDI) if **4** were to be co-administered with a prototypical OAT1 substrate/inhibitor, such as probenecid.

Figure 5. GSK126 (1.0 μM) time-dependent (1, 5 and 10 min) uptake into S2 and S2-hOAT expressing cell lines; ■ = S2-mock, ▲ = S2-hOAT1, ▼ = S2-hOAT2, ♦ = S2-hOAT3, and ● = S2-hOAT4; n = 4 ± SD; * = P < 0.01.

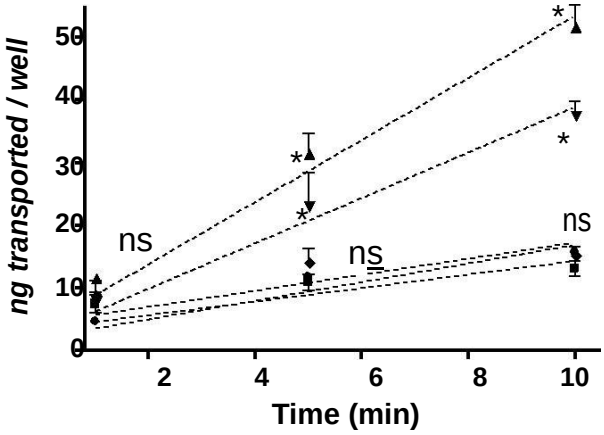

We next sought to implement a series of rat PK studies employing tail-vein blood collections as follows: i) oral capsule dosing of GSK126 (20% drug loading) followed by a water bolus (500 □L), n = 4; ii) oral gavage suspension dosing (**4**; 50 mg/kg dose, n = 3); iii) Orbital Sinus Dosing (OSD) of **4** (1.0 mg/kg, n = 4); iv) OSD (1.0 mg/kg) followed by organ harvesting in order to obtain fundamental tissue distribution data, n = 4; v) probenecid (i.p. 20 mg/kg) followed by OSD (**4**; 1.0 mg/kg; 15 min post-dose) to probe potential DDI, n = 4; and v) OSD of **4** with urine collection via metabolic cages, n = 4. In the case of the oral capsule (7.0 mg/kg) dosing, we could only detect trace amounts of **4** in the collected blood samples (data not shown). In contrast, when we administered an oral gavage suspension (i.e. in part circumventing a distinct dissolution issue via packed capsule experiments), we could detect parent drug substance in the circulating blood over time (**Figure 6A**). The oral dose (**4**, 50 mg/kg; n=3) data produced the

Figure 6A. GSK126 oral gavage dosing (50 mg/kg) to male Sprague-Dawley rats; tail vein blood samples versus time profile (n = 3 ± SD), 0 – 8 h data (24 h time-point not shown for representative clarity).

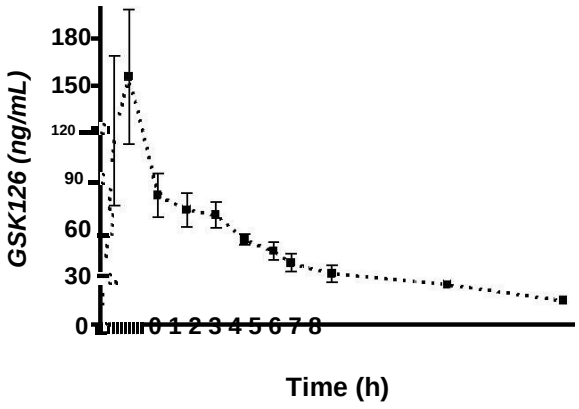

following PK parameters: an AUC0-∞ = 636.3 ± 82.0 h•ng/mL, Cmax 155.6 ± 42.4 ng/mL, Tmax = 0.25 h, and elimination T1/2 = 10.7 ± 3.2 h. Two sets of OSD experiments were then conducted (**Figure 6B**) to i) allow us to determine the observed oral bioavailability computed via Fa = AUCoral * OSD (mg/kg) / AUCOSD * oral dose (mg/kg); and ii) to probe for potential OAT mediated *in vivo* DDI which may exist as per the *in vitro* OAT results (**Figure 5**). The OSD group (**4** at 1.0 mg/kg; n = 4) afforded the following PK values: AUC0-∞ = 1012.4 ± 213.8 h•ng/mL and elimination T1/2 = 3.2 ± 0.3 h. Whereas the OSD group (**4** at 1.0 mg/kg; n = 3) – which was dosed 15 min after the probenecid dose (20 mg/kg i.p.) – produced the following PK data: AUC0-∞ = 1259.6 ± 394.4 h•ng/mL and elimination T1/2 = 3.6 ± 0.4 h (**Figure 6B**). So, while a visual inspection of the plotted data (**Figure 6B**) may appear that these two PK profiles are different, the comparisons were not statistically significant; P = 0.4312 and P = 0.3727 for AUC and T1/2 comparisons, respectively. Hence, while we may have observed **4** to be an OAT1 and OAT2 substrate, the presence of the prototypical OAT inhibitor probenecid did not readily alter the observed *in vivo* blood versus time profile.

Figure 6B. GSK126 orbital sinus dosing (1.0 mg/kg) and blood versus time (2-240 min) profile, ■ = GSK126 (n = 4 ± SD), ▲ = GSK126 and probenecid (20 mg/kg i.p.).

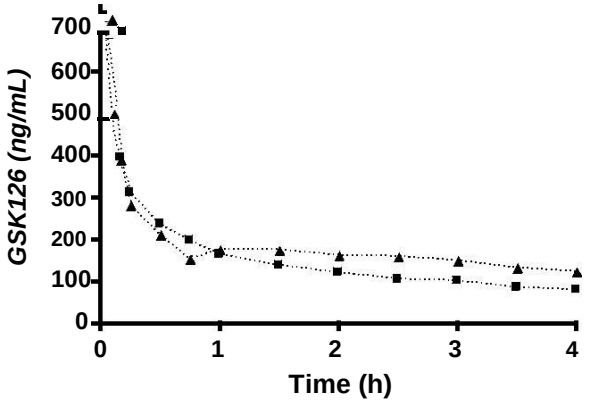

Conclusion

The oral (**Figure 6A**) and OSD (**Figure 6B**) data demonstrate that the oral bioavailability of **4** via our experiments was < 2%. These results demonstrate that **4** has poor solubility/dissolution; factors which may potentially be improved via formulation (*i.e.* solubility enhancers and/or dissolution control) development, but was not a goal of the current work. Thereafter, we performed another set of orbital sinus dosing experiments with the goal to sacrifice the animals, collect organs, homogenize, analyze and produce tissue distribution data. As summarized in **Figure 7**, the reported tissue values were at the time that drug blood concentrations were between 102.5 ± 25.7 ng/mL (essentially 2.0 h post-OSD in **Figure 6B**). These OSD data illustrate that GSK126 **4** can cross the blood-brain barrier (BBB), brain concentration of **4** ranged between 70.5 ± 9.9 ng/g. Furthermore, **4** was shown to predominately distribute to liver and kidney. Lastly, we conducted a set of experiments and dosed animals (OSD, 1.0 mg/kg; n = 4) and collected urine (0-8 h time frame). Consistent with the tissue distribution data (**Figure 7**), we were able to detect **4** and the three Phase I metabolites **L-**

M1, **L-M2**, and **L-M3** in rat urine; the observed concentrations (0 – 8 h) were 1347.3 ± 204.4 ng/mL, 5.6 ± 0.4 ng/mL, 2.8 ± 0.1 ng/mL, and 4.6 ± 0.2 ng/mL, respectively.

These data illustrate that GSK126 **4** can cross the BBB, and Phase I oxidative metabolites formed via liver are eliminated, in part, via renal excretion. Consequently, the PK and tissue distribution data generated from the current experiments provide us with important ADME information to guide dosing (dose and frequency) as we conduct *in vivo* tumor model studies; experiments to be performed in the presence and absence of potent LAT1 inhibitor(s), and other cancer drugs (*e.g.* rapamycin, doxorubicin, etc.) with the goal to establish, or not, *in vitro* – *in vivo* (IV-IV) synergistic correlations predicted from our cell based experiments. The ability to establish when and when not to use multi-drug therapy treatments to treat various cancers (i.e. kidney, colon, liver) is needed and thus future efforts to probe synergistic, or additive, effects is warranted.

Figure 7. GSK126 and metabolite (**L-M1**, **L-M2**, and **L-M3**) concentrations observed in tissue (brain, kidney, liver), data represented as ng/g tissue, n = 4 ± SD.

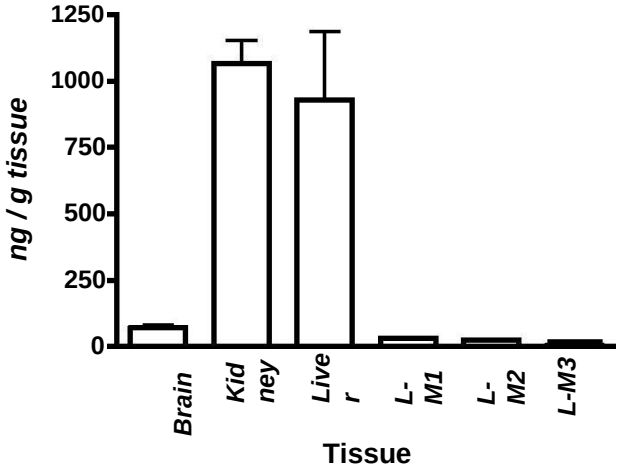

3. Experimental

3.1 Materials and Methods

Acetic acid, acetonitrile (ACN), diethyl ether, dimethylformamide (DMF), dimethyl sulfoxide (DMSO), 1,4-dioxane, ethyl acetate (EtOAc), EDTA, hexanes, hydrochloric acid (HCl), isopropanol, methanol (MeOH), magnesium chloride (MgCl2), methylene chloride (DCM), petroleum ether, potassium carbonate (K2CO3), potassium phosphate (tribasic), sodium acetate, sodium bicarbonate (NaHCO3), sodium chloride (NaCl), sodium hydride (NaH), sodium hydroxide (NaOH), anhydrous sodium sulfate (Na2SO4), triethyl amine (TEA) and water (H2O) were purchased from Fisher Scientific (Pittsburgh, PA). Acetyl acetone, (*S*)-(+)-2-butanol, carboxy-methyl cellulose sodium (CMC), celite, chloroacetamide, cyano-acetamide, deuterated acetic acid, deuterium oxide (D2O), deuterated chloroform (CDCl3), deuterated dimethyl sulfoxide (DMSO-*d6*), 1,3-dibromo-5,5 dimethyl -2,4-imadazolidinedione, (*N*-(3-dimethylaminopropyl)-*N′*-ethylcarbodiimide (EDC), *N*,*N*-dimethylformamide dimethyl acetal (DMF-DMA), fetal calf serum (FCS), formic acid, 1-hydroxy-7-azabenzotriazole (HOAT), *N*-methylmorpholine, 2-methyl-3-nitro benzoic acid, nicotinamide adenine dinucleotide phosphate (NADPH), palladium on carbon (10%), penicillin, platinum oxide, [1,1′-bis(diphenylphosphino)ferrocene] dichloropalladium (II) complex with dichloromethane (PdCl2(dppf)-DCM), phosphorus tribromide, phosphoryl trichloride, ^{13}C-enriched potassium cyanide, sodium pyruvate, streptomycin, 1-(5-(4,4,5,5-tetramethyl-1,3,2-dioxaborolan-2-yl)pyridin-2-yl)piperazine, *p*-tolunesulfonyl hydrazide, *p*-toluene-sulfonic acid monohydrate, sulfolane, and sodium cyano-borohydride were obtained from Sigma-Aldrich Chemical Company (St. Louis, MO). Nitrogen gas and hydrogen gas were procured from AirGas® (Denver, CO). Ethanol was purchased from Decon Laboratories, Inc. (King of Prussia, PA). Reactions were monitored via silica gel IB2-F thin layer chromatography (TLC) plates from J.T. Baker (Phillipsburg, NJ). Silica Gel 60 Å 40-63 □m was purchased from Sorbent Technologies (Norcross, GA). SD rat microsomes (liver, Lot # 1010122, pool of 400) were acquired from Xenotech LLC (Kansas City, KS). RPMI 1640 medium was procured from Invitrogen (Grand Island, NY). Control tissues – male rat whole blood (K2 EDTA), plasma (K2 EDTA), livers, kidneys, and brains – were procured from Bioreclamation LLC (Westbury, NY). The ^{1}H and ^{13}C NMR spectra were recorded using a 400 MHz Bruker NMR, Avance III 400. The chemical shifts are reported in ppm. An Applied Biosystems Sciex 4000 (Applied Biosystems; Foster City, CA) was equipped with a Shimadzu HPLC (Shimadzu Scientific Instruments, Inc.; Columbia, MD) and Leap auto-sampler (LEAP Technologies; Carrboro, NC) was used to perform the BioAnalytical PharmacoKinetic (BAPK) analysis and establish tissue distribution data.

3.2 GSK126 Synthesis (Scheme 1):

3.2.1 5-Bromo-2-methyl-3-nitrobenzoic acid; 8: 2-Methyl-3-nitro benzoic acid (100 g, 552 mmol) was weighed into a round bottom flask (RBF) containing a stir-bar and concentrated sulfuric acid (H2SO4; 500 mL) was slowly added followed by 1,3-dibromo-5,5 dimethyl -2,4-imadazolidinedione (86.8 g, 304 mmol). The reaction mixture was stirred at room temperature (5.0 h) and then slowly poured into ice water (2.0 L) to afford a precipitant. The solid was then Büchner filtered and washed with ice cold water (1.2 L) followed by petroleum ether (1.0 L). The solid was

dried to afford the brominated benzoic acid as a white solid (**8**; 132 g, 92% yield) and used without further purification. ^{1}H NMR (DMSO-*d6*, 400 MHz): δ ppm 8.30-8.29 (d, 1H), 8.14-8.13 (d, 1H), 6.37 (bs, 1H), 2.44 (s, 3H).

3.2.2 Methyl 6-bromo-1H-indole-4-carboxylate; 9: To a stirred solution of 5-bromo-2-methyl-3-nitrobenzoic acid (**8**; 10.0 g, 38.5 mmol) in DMF (40 mL) was added *N*,*N*-dimethylformamide dimethyl acetal (DMF-DMA) (46.0 mL, 346 mmol) at room temperature. The reaction mixture was refluxed (110-120 ^{o}C, 18 h), allowed to cool to ambient temperature and then concentrated under reduced pressure. The residue was dissolved in acetic acid (50 mL) and then added in portions to a suspension of iron (23.6 g, 423 mmol) in acetic acid (100 mL; 50 ^{o}C). The reaction mixture was stirred (80-90 ^{o}C; 4 h) and then filtered through a plug of Celite. The filtrate was poured onto ice water and extracted with ethyl acetate. The combined organic layers were washed with sat. NaHCO3, brine, dried over anhydrous Na2SO4, filtered, and concentrated under reduced pressure. The crude product was purified by silica gel chromatography using CH2Cl2–MeOH (10:1) as an eluent to afford indole (**9**, 5.10 g, 52% yield) as a solid compound. ^{1}H NMR (DMSO-*d6*, 400 MHz): δ ppm 11.6 (bs, 1H), 7.86-7.85 (d, 1H), 7.77-7.76 (d, 1H), 7.57-7.56 (d, 1H), 6.93-6.92 (d, 1H), 3.89 (s, 3H).

3.2.3 (R)-(-)-2-butyl bromide, 10: (*S*)(+)2-Butanol (5.00 g, 67.5 mmol) was stirred (0 ^{o}C) while phosphorus tri-bromide (6.98 mL, 74.2 mmol) was slowly added and the contents stirred (24 h). The reaction mixture was then warmed (~50 ^{o}C) and poured into a mixture of diethyl ether and saturated aqueous NaHCO3. The aqueous phase was extracted with diethyl ether, and the combined organic extracts were dried over anhydrous Na2SO4, filtered, and concentrated to afford chiral alkyl halide (**10**, 6.0 g, 65% yield) as a liquid. ^{1}H NMR (CDCl3, 400 MHz): δ ppm 3.75-3.67 (m, 1H), 1.52-1.41 (m, 2H), 1.18-1.16 (d, 3H), 0.94-0.89 (t, 3H).

3.2.4 (S)-Methyl 6-bromo-1-sec-butyl-3-methyl-1H-indole-4-carboxylate, 11: To a stirred solution of indole (**9**; 5.00 g, 19.2 mmol) in anhydrous DMF (75.0 mL) was added NaH (692 mg, 28.9 mmol) at 0 ^{o}C. Next, alkyl halide (**10**, 5.27 g, 38.5 mmol) was added to the reaction mixture, stirred (10 min), allowed to warm to room temperature and stirred (18 h). The reaction mixture was then quenched by adding cold water and the contents extracted with ethyl acetate, dried over anhydrous Na2SO4, filtered, and concentrated under reduced pressure. The crude product was purified by silica gel chromatography using hexane:CH2Cl2 (10:1) to give (*S*)-butyl indole (**11**, 2.20 g, 36% yield) as a liquid compound. ^{1}H NMR (CDCl3, 400 MHz): δ ppm 7.99-7.98 (d, 1H), 7.71 (s, 1H), 7.31-7.29 (d, 1H), 7.14-7.12 (d, 1H), 4.40-4.32 (m, 1H), 3.98 (s, 3H), 1.91-1.85 (m, 2H), 1.52-1.50 (d, 3H), 0.85-0.81 (t, 3H).

3.2.5 (S)-Methyl 6-bromo-1-sec-butyl-3-formyl-1H-indole-4-carboxylate, 12: To a solution of DMF (30 mL) was added POCl3 (80.0 □L, 8.51 mmol) at 0 ^{o}C and stirred (20 min). Next, (**11**, 2.20 g, 7.09 mmol) in DMF (20 mL) was added to the reaction mixture at 0 ^{o}C. The reaction mixture was allowed to warm at room temperature and stirred (3.0 h). The reaction mixture was then diluted with ice cold water and pH adjusted (~8.0 with 2.0 N NaOH aq.) and extracted with ethyl acetate. The organic layer was washed with brine, dried over anhydrous Na2SO4, filtered, and concentrated under reduced pressure to give (**12**, 2.10 g, 88% yield) as a solid compound. The compound was used without further purification. ^{1}H NMR (CDCl3, 400 MHz): δ ppm 10.4 (s, 1H), 8.07 (s, 1H), 7.94-7.93 (d, 1H), 7.75-7.74 (d, 1H), 4.46-4.36 (m, 1H), 3.99 (s, 3H), 1.98-1.88 (m, 2H), 1.56-1.54 (d, 3H), 0.89-0.85 (t, 3H).

3.2.6 (S)-Methyl 6-bromo-1-sec-butyl-3-methyl-1H-indole-4-carboxylate, 13: To a stirred solution of (**12**, 2.00 g, 5.91 mmol) at room temperature in DMF (20 mL) was added *p*-toluene- sulfonic acid monohydrate (147 mg, 0.77 mmol) and *p*-tolunesulfonyl hydrazide (1.43 g, 7.68 mmol). Next, sulfolane (20 mL) was added and the reaction mixture stirred (100 ^{o}C; 1.0 h). The contents were allowed to cool to room temperature and sodium cyano-borohydride (1.49 g, 23.6 mmol) was added in portions over 25 min. The reaction mixture was stirred at 100 ^{o}C (2.0 h), cooled to ambient temperature and stirred (16 h). Next, the mixture was diluted with water and extracted with 20% ethyl acetate:hexane. The organic layer was washed with water, brine, dried over anhydrous Na2SO4, filtered, and concentrated under reduced pressure. The crude material was purified by silica gel chromatography using hexane:CH2Cl2 (1:1) as an eluent to give (**13**, 1.80 g, 94% yield) as a solid compound. ^{1}H NMR (CDCl3, 400 MHz): δ ppm 7.68-7.67 (d, 1H), 7.62-7.61 (d, 1H), 7.04 (s, 1H), 4.33-4.24 (m, 1H), 3.95 (s, 3H), 2.37 (s, 3H), 1.90-1.78 (m, 2H), 1.47-1.45 (d, 3H), and 0.84-0.80 (t, 3H).

3.2.7 (S)-6-bromo-1-sec-butyl-3-methyl-1H-indole-4-carboxylic acid, 14: To a stirred solution of (**13**, 1.50 g, 4.63 mmol) in ethanol (40 mL) was added 1.0 N NaOH (5.0 mL). The reaction mixture was heated (90 ^{o}C; 6.0 h), allowed to cool, and concentrated under reduced pressure. The residue was diluted with water, acidified with 1.0 N HCl, and extracted with ethyl acetate. The organic layers were combined, dried over anhydrous Na2SO4, filtered, and concentrated under reduced pressure to afford acid **14** as a white solid (1.40 g, 98% yield). ^{1}H NMR (CDCl3, 400 MHz): δ ppm 11.9 (bs, 1H), 7.90-7.89 (d, 1H), 7.68-7.67 (d, 1H), 7.08 (s, 1H), 4.36-4.27 (m, 1H), 2.46 (s, 3H), 1.92-1.80 (m, 2H), 1.49-1.47 (d, 3H), and 0.86-0.81 (t, 3H).

3.2.8 Methyl 6-bromo-3-formyl-1H-indole-4-carboxylate, 15: To a solution of DMF (60 mL; 0 ^{o}C) was added POCl3 (2.21 mL, 23.6 mmol) and stirred (20 min). Next, (**9**, 5.00 g, 19.7 mmol) in DMF (40 mL; 0 ^{o}C) was added. The contents were allowed to warm to ambient temperature and stirred (3.0 h). The reaction mixture was diluted with ice cold water and the pH was adjusted to ~8.0 with 2.0 N NaOH and then the mixture was extracted with ethyl acetate. The organic layer was washed with brine, dried over anhydrous Na2SO4, filtered, and concentrated under reduced pressure to afford (**15**, 5.00 g, 92% yield) as a solid compound. The compound was subsequently used without further purification. ^{1}H NMR (DMSO-*d6*, 400 MHz): δ ppm 12.6 (bs, 1H), 10.1 (s, 1H), 8.35 (s, 1H), 7.92-7.91 (d, 1H), 7.63-7.62 (d, 1H), 3.85 (s, 3H).

3.2.9 Methyl 6-bromo-3-methyl-1H-indole-4-carboxylate, 16: To a stirred solution of (15, 5.00 g, 17.7 mmol) in DMF (40 mL) was added at room temperature *p*-tolunesulfonic acid monohydrate (438 mg, 2.30 mmol), *p*-tolunesulfonyl hydrazide (4.28 g, 23.0 mmol), and sulfolane (40 mL). The reaction mixture was heated with stirring (100 ^{o}C; 1.0 h). The contents were allowed to cool to ambient temperature and then sodium cyano-borohydride (4.45 g, 70.8 mmol) was added in portions over a period of 25 min. Next, the reaction mixture was heated and stirred (100 ^{o}C; 2.0 h), and then allowed to cool to ambient temperature and stirred (16 h). The reaction was diluted with water and extracted (20% ethyl acetate:hexane). The organic layers were combined and washed with water, brine, dried over anhydrous Na2SO4, filtered and concentrated under reduced pressure. The crude material was purified by silica gel chromatography using hexane:CH2Cl2 (1:1) as an eluent to afford (**16,** 3.50 g, 74% yield) as a yellow solid. ^{1}H NMR (DMSO-*d6*, 400 MHz): δ ppm 11.3 (bs, 1H), 7.73-7.72 (d, 1H), 7.50-7.49 (d, 1H), 7.31 (s, 1H), 3.85 (s, 3H), 2.56 (s, 3H).

3.2.10 (S)-methyl 6-bromo-1-sec-butyl-3-

methyl-1H-indole-4-carboxylate, 13: To a stirred solution of (**16**, 3.00 g, 11.2 mmol) in DMF (35 mL) was added sodium hydride (403 mg, 16.8 mmol) at 0 ^{o}C. Next, (**10**, 3.07 g, 22.4 mmol) was added drop-wise to the reaction mixture, stirred (10 min), and the reaction allowed to warm to ambient temperature and stirred (18 h). The reaction mixture was quenched with ice cold water and extracted with ethyl acetate. The organic phase was dried over anhydrous Na2SO4, filtered, and concentrated under reduced pressure. The crude product was purified by silica gel chromatography using hexane:CH2Cl2 (10:1) as an eluent to afford (**13**, 1.60 g, 44% yield).

3.2.11 (S)-6-bromo-1-sec-butyl-3-methyl-1H-indole-4-carboxylic acid, 14: To a stirred solution of (**13**, 1.50 g, 4.63 mmol) in ethanol (40 mL) was added 1.0 N NaOH (5.0 mL). The reaction mixture was heated (90 ^{o}C; 6.0 h), allowed to cool, and concentrated under reduced pressure. The residue was diluted with water, acidified with 1.0 N HCl, and extracted with ethyl acetate. The organic layers were combined, dried over anhydrous Na2SO4, filtered, and concentrated under reduced pressure to afford acid **14** as a white solid (1.40 g, 98% yield). ^{1}H NMR (CDCl3, 400 MHz): δ ppm 11.9 (bs, 1H), 7.90-7.89 (d, 1H), 7.68-7.67 (d, 1H), 7.08 (s, 1H), 4.36-4.27 (m, 1H), 2.46 (s, 3H), 1.92-1.80 (m, 2H), 1.49-1.47 (d, 3H), and 0.86-0.81 (t, 3H).

3.2.12 4,6-Dimethyl-2-oxo-1,2 dihydropyridine-3-carbonitrile, **17**: Cyano-acetamide (100 g, 1.19 mol) was dissolved in absolute ethanol (500 mL) and an aqueous solution of potassium carbonate (163 g, 1.19 mol) was then added followed by acetyl acetone (122 mL, 1.19 mol). The reaction mixture was stirred at room temperature (16 h) and then water was added and the contents extracted with ethyl acetate. The organic phase was dried over anhydrous Na2SO4, filtered, and concentrated under reduced pressure to afford nitrile **17** as a white solid (141 g, 80% yield) as a white solid compound. ^{1}H NMR (DMSO-*d6*, 400 MHz): δ ppm 6.11 (s, 1H), 5.00 (bs, 1H), 2.28 (s, 3H), 2.21 (s, 3H).

3.2.13 3-(Aminomethyl)-4,6-dimethylpyridin-2(1H)-one hydrochloride salt, 18: Palladium on carbon (10%) (1.08 g) was charged into a 500 mL dry Parr bottle and a small amount of acetic acid (1.0 mL) was added. Next, compound (**17**, 10.0 g, 67.5 mmol), sodium acetate (10.3 g, 125 mmol), platinum oxide (72.6 mg) and acetic acid (300 mL) were added. The bottle was capped, placed onto a Parr apparatus and shaken under H2 (100 psi; 16 h). Next, the reaction mixture was gravity filtered and the solvent removed under reduced pressure to afford a residue which was treated with concentrated HCl (25 mL) to produce solid material which was filtered. The yellow filtrate was then concentrated under reduced pressure and concentrated HCl (20 mL) and ethanol (50 mL) were added, cooled to 0 ^{o}C, stirred (cold, 2.0 h) and the solid was filtered, washed with ice cold ethanol, diethyl ether and dried to afford (**18**, 8.30 g 65% yield) as a white solid. ^{1}H NMR (DMSO-*d6*, 400 MHz): δ ppm 11.8 (bs, 1H), 8.09 (bs, 3H), 5.94 (s, 1H), 3.76-3.71 (m, 2H), 2.20 (s, 3H), 2.14 (s, 3H).

3.2.14 (S)-6-Bromo-1-sec-butyl-N-((4,6-dimethyl-2-oxo-1,2-dihydropyridin-3-yl)methyl)-3-methyl-1H-indole-4-carboxamide, 19: Added sequentially to a reaction flask under a nitrogen environment were: (**14**, 1.50 g, 4.84 mmol), (**18**, 1.37 g, 7.26 mmol), 1-hydroxy-7-azabenzotriazole (HOAT, 0.99 g, 7.26 mmol), and EDC (N-(3-dimethylaminopropyl)-N′-ethylcarbodiimide; 1.39 g, 7.26 mmol) followed by DMSO (30 mL via syringe transfer) and *N*-methylmorpholine (2.13 mL, 19.4 mmol via syringe transfer). The contents were stirred at room temperature (24 h) under nitrogen and the solids

gradually dissolved. Next, the reaction mixture was slowly diluted into ice cold water and stirred (10 min) and then allowed to stand unstirred (10 min). The contents were Büchner filtered, the solid washed with water, and dried to produce a white solid (**19**, 1.70 g, 79% yield). ^{1}H NMR (DMSO-*d6*, 400 MHz): δ ppm 11.4 (bs,1H), 8.22-8.20 (t, 1H), 7.75-7.74 (d, 1H), 7.28 (s, 1H), 6.98-6.97 (d, 1H), 5.84 (s, 1H), 4.51-4.42 (m, 1H), 4.29-4.28 (d, 2H), 2.20 (s, 3H), 2.11 (s, 3H), 2.10 (s, 3H), 1.79-1.71 (m, 2H), 1.36-1.34 (d, 3H), 0.70-0.66 (t, 3H).

3.2.15 (S)-1-sec-butyl-N-((4,6-dimethyl-2-oxo-1,2-dihydro-pyridin-3-yl)methyl)-3-methyl-6-(6-(piperazin-1-yl)pyridin-3-yl)-1H-indole-4-carboxamide (GSK126; **4)**: To a sealed-vial containing a stir bar were added (**17**, 1.50 g, 3.38 mmol), 1-(5-(4,4,5,5-tetramethyl-1,3,2-dioxaborolan-2-yl)pyridin-2-yl)piperazine (1.27 g, 4.39 mmol), potassium phosphate (tribasic) (2.87 g, 13.5 mmol) followed by 1,4-dioxane (35 mL) and water (7.0 mL). The suspension was stirred under nitrogen (degassing for 10 min) and then PdCl2(dppf)-DCM (277 mg, 0.338 mmol) was added. The reaction vessel was sealed, placed into an oil bath (100 ^{o}C) and stirred (1.5 h). Next, the reaction vessel was removed from heat and allowed to cool to ambient temperature. Theaqueous layer was removed from the reaction vial via pipette transfer. The organic phase was then concentrated under reduced pressure and the crude material purified on a silica gel column using CH2Cl2-(1% triethylamine MeOH) (10:1) as an eluent to afford GSK126 (**4**; 1.50 g, 84% yield) as an off white solid compound. ^{1}H NMR (DMSO-d6, 400 MHz): δ ppm 11.4 (bs, 1H), 8.48-8.47 (d, 1H), 8.13-8.11 (t, 1H), 7.90-7.87 (dd, 1H), 7.70 (d, 1H), 7.23 (s, 1H), 7.15 (d, 1H), 6.87-6.84 (d, 1H), 5.85 (s, 1H), 4.61-4.53 (m, 1H), 4.34-4.33 (d, 2H), 3.43-3.40 (m, 4H), 2.79-2.76 (m, 4H), 2.22 (m, 3H), 2.14 (s, 3H), 2.10 (s, 3H), 1.82-1.74 (m, 2H), 1.39-1.44 (d, 3H), 0.73-0.69 (t, 3H).

^{13}C NMR (DMSO-d6, 100 MHz): δ ppm 169.2 (CO), 163.6 (CO), 158.7 (C), 149.8 (C), 146.0(CH), 143.1 (C), 138.2 (C), 136.3 (CH), 131.1 (C), 130.2 (C), 126.5 (C), 124.8 (CH), 123.4 (C), 122.2 (C), 116.5 (CH), 110.2 (C), 108.1 (CH), 107.9 (CH), 107.2 (CH), 52.1 (CH), 46.4 (2 CH2), 45.8 (2 CH2), 35.5 (CH2), 30.0 (CH2), 21.3 (CH3), 19.4 (CH3), 18.6 (CH3), 12.1 (CH3), 11.2 (CH3). These NMR results for **4** are consistent with previously reported data (McCabe et al. 2012).

3.3 Internal Standard (IS) GSK126-d7 Synthesis (Scheme 2):

3.3.1 Acetyl acetone-d8, 20: To a D2O solution (20 mL) containing acetyl acetone (2.0 g) was added potassium carbonate (0.40 g, 2.9 mmol). The reaction mixture was heated (120 ^{o}C; 16 h) and then the reaction mixture was extracted with DCM, dried over anhydrous Na2SO4, filtered, and concentrated under reduced pressure to afford deuterated acetyl acetone which was determined to be ~90% deuterated as determined via ^{1}H NMR. To fully incorporate deuterium, the isolated material was subjected to a second round of the above reaction conditions to afford **20** (1.1 g, 51% yield) which did not exhibit any protons via ^{1}H NMR analysis (CDCl3, 400 MHz).

3.3.2 4,6-Dimethyl-2-oxo-1,2-dihydropyridine-3-carbonitrile-d8, 21: Cyanoacetamide (389 mg, 4.62 mmol) was dissolved in ethanol-d (20 mL) and a solution of potassium carbonate in D2O (639 mg, 4.62 mmol in 1.0 mL D2O) was added. Next, (**20**, 500 mg, 4.62 mmol) was added and the reaction was stirred (16 h). Next, D2O was added and the mixture extracted with ethyl acetate. The organic was dried over anhydrous Na2SO4, filtered, and concentrated under reduced pressure to afford deuterated (**21**, 250 mg, 35% yield) as a solid compound.

3.3.3 3-(Aminomethyl)-4,6-dimethylpyridin-2(1H)-one-d7 hydrochloride salt, 22: Palladium on charcoal (10%) (40 mg) was charged into a 250 mL dry Parr bottle and a small amount

of acetic acid-d (0.5 mL) was added. Next, deuterated (**21**, 200 mg, 1.28 mmol), sodium acetate (200 mg, 2.43 mmol), platinum oxide (8.0 mg) and acetic acid-d (20 mL) were added. The bottle was capped, placed onto the Parr apparatus, and shaken under hydrogen (100 psi; 16 h). The reaction mixture was then gravity filtered and the filtrate removed under reduced pressure to afford a residue which was treated with concentrated HCl (20 mL) and the solids thus formed were filtered; the addition of HCl effectively produces a deuterium hydrogen exchange that the resulting product was now incorporated with seven deuterium atoms, not eight. The yellow filtrate was concentrated under reduced pressure and diluted with concentrated HCl (10 mL) and ethanol (300 mL). The mixture was cooled (0 ^{o}C; 2.0 h) and the solid thus formed filtered, washed with ice cold ethanol, diethyl ether, and dried to produce **22** as a white solid (160 mg; 79% yield). ^{1}H-NMR (DMSO-*d6*, 400 MHz): δ ppm 12.3 (bs, 1H), 8.04 (bs, 3H), 3.75-3.72 (m, 2H).

3.3.4 (S)-6-bromo-1-sec-butyl-N-((4,6-dimethyl-2-oxo-1,2-dihydropyridin-3-yl)methyl)-3-methyl-1H-indole-4-carboxamide-d7 23: To a RBF containing a stir-bar under N2 was added (**14**; 527 mg, 1.70 mmol), (**22**; 500 mg, 2.55 mmol), 1-hydroxy-7-azabenzotriazole (HOAT, 347 mg, 2.55 mmol), and EDC (489 mg, 2.55 mmol). Next, DMSO (15 mL) and *N*-methylmorpholine (0.75 mL, 6.8 mmol) were added via syringe transfer. The contents were stirred at room temperature (24 h) while the solids gradually dissolved. The reaction contents were slowly diluted into ice water, stirred (10 min), and then allowed to stand unstirred (10 min). The reaction was filtered and the solid was washed with water, dried over anhydrous Na2SO4, filtered, and concentrated under reduced pressure to afford deuterated (**23**, 450 mg, 59% yield) as a white solid compound. ^{1}H NMR (CDCl3, 400 MHz): δ ppm 12.3 (bs, 1H), 7.47 (d, 1H), 7.20 (s, 1H), 7.17-7.15 (m, 1H), 6.92 (d, 1H), 4.60-4.55 (d, 2H), 4.29-4.22 (m, 1H), 2.23 (s, 3H), 1.85-1.78 (m, 2H), 1.44-1.42 (d, 3H), 0.84-0.78 (t, 3H); ^{13}C NMR (CDCl3, 100 MHz): δ ppm 168.3, 165.4, 150.7,142.9, 138.5, 138.1, 131.4, 124.2, 123.3, 121.7, 120.5, 113.8, 113.6, 110.9, 53.0, 40.1, 36.1, 30.0, 20.9, 13.3, 11.6, and 10.9.

3.3.5 (S)-1-sec-butyl-N-((4,6-dimethyl-2-oxo-1,2-dihydro pyridin-3-yl)methyl)-3-methyl-6-(6-(piperazin-1-yl) pyridin-3-yl)-1H-indole-4-carboxamide-d7 (GSK-d7, **24:** To a reaction vial were sequentially added the following: (**23**, 400 mg, 0.89 mmol), 1-(5-(4,4,5,5-tetramethyl-1,3,2-dioxaborolan-2-yl)pyridin-2-yl)piperazine (289 mg, 1.16 mmol) and potassium phosphate (tribasic) (756 mg, 3.56 mmol) followed by 1,4-dioxane (10 mL) and water (3.0 mL). The suspension was stirred and degassed under nitrogen (10 min). Next, PdCl2(dppf)-DCM adduct (72.9 mg, 0.089 mmol) was added, the reaction vessel was sealed and placed into oil bath (100 ^{o}C; stirred 1.5 h). The contents were allowed to cool to ambient temperature and the aqueous layer removed via pipette transfer. The organic layer was then concentrated under reduced pressure and the crude material was purified by silica gel chromatography using CH2Cl2-(1% triethyl amine in MeOH) (10:1) as an eluent to produce deuterated analog (**24**; GSK-d7, 100 mg, 32% yield) as an off white solid. ^{1}H NMR (CDCl3, 400 MHz): δ ppm 10.2 (bs, 1H), 8.38 (d, 1H), 7.67-7.64 (dd, 1H), 7.40 (d, 1H), 7.23 (d, 1H), 7.21 (s, 1H), 6.96 (d, 1H), 4.57-4.55 (d, 2H), 4.38-4.32 (m, 1H) 3.66-4.64 (m, 4H), 3.11-3.07 (m, 4H), 2.23 (s, 3H), 1.85-1.78 (m, 2H), 1.45-1.43 (d, 3H), and 0.81-0.77 (t, 3H).

3.4 Verification of in vitro biological activity

3.4.1 D283 cell viability: Medulloblastoma cell line (**Figure 2A**) known as D283 (purchased from ATCC)

was used; passage less than 20. The D283 cells were plated (50,000 cells per well) in Corning Costar 24 well plates (#3524). The D283 cells were plated in 1.5 mL Gibco DMEM medium supplemented with 10% FBS and dilutions of GSK126 suspended in DMSO were performed; final DMSO concentration did not exceed 0.2%. At time of harvest, the cell suspensions were transferred to 1.5 mL micro-centrifuge tubes which were pelleted at 1,000 x g (5 min), the supernatant was aspirated and the cell pellets resuspended in 0.5 mL of Accutase Cell Detachment Solution to disaggregate the cells. The single cell suspensions were then pelleted at 1000 x g (5 min), the supernatant was aspirated and then the cells were resuspended in phosphate buffered saline. A 100 mL aliquot was taken and added to 100 mL of Guava ViaCount reagent and analyzed on a Guava EasyCyte Plus flow cytometer to determine the number of total cells per mL for each treatment as previously described (Harris et al., 2012).

3.4.2 D283 cells and Western blot analysis: D283 medulloblastoma cells were treated with different concentration of **4** (**Figure 2B**) for 3 days and histones were acid extracted following modified Abcam's histone extraction protocol previously described (Alimova et al., 2012). The cell pellet was re-suspended in PBS buffer containing 0.5% triton X 100 (v/v) and cells lysed on ice (15 min). This was centrifuged at maximum speed (10 min; 4°C). The cell pellet was again resuspended in 50 uL of the PBS buffer containing Triton X. Centrifuged and the supernatant was discarded. This cell pellet was then resuspended in 0.2N HCl (100 uL for one million cells) and left overnight at 4°C. Next day, the cell suspension was centrifuged at maximum speed and the supernatant containing the histones was examined for the expression of histones by western blotting. The standard procedure was performed with a rabbit anti-H3K27Me3 and anti-H3 antibodies (Active Motif) (Alimova et al., 2013).

3.4.3 tPTEN-/- cell line KO99L: *Pten*-deficient mice (tPTEN-/-) were bred by crossing mice carrying two *Pten* floxed alleles with proximal lck promoter-cre transgenic mice and characterized via PCR as previously described (Hagenbeek et al., 2004). Mice and derived tPTEN-/- cell line KO99L was established as previously described (Rosilio et al., 2015). The murine KO99L cell line was grown in RPMI 1640 medium supplemented with 20% Fetal Calf-Serum and penicillin (50 units/mL), streptomycin (50 mg/mL) and sodium pyruvate (1.0 mM) Cell cultures were maintained at 37°C under 5% CO2.

3.4.4 Measurement of KO99L cell metabolism (WST-1) and viability: KO99L cells (40,000 cells per 100 µL) were incubated with **4** in a 96-well plate format for 48 h (37°C). Ten microliters

of WST-1 reagent was added to each well and the absorbance of the formazan product was measured (490 nm). Each assay was performed in quadruplicate. Cells (5.0 x 10^5 cells per 2.0 mL) were incubated in a 6-well plate with indicated concentration of **4**, collected, washed twice with PBS and re-suspended with a staining solution containing DAPI (4',6'-diamidino-2-phenylindole) (0.5 µg/mL) and immediately analyzed by flow cytometry (MacsQuant Analyser, Miltenyi Biotech SA, Paris, France). Hence, cell viability was assessed using a WST-1 assay (evaluates mitochondrial dehydrogenase activity), whereas survival was quantified through DAPI incorporation.

3.4.5 Rat liver microsomal in vitro metabolism: To probe the *in vitro* metabolism of **4**, rat liver microsomal incubations were conducted following analogous procedures as previously described (Wempe et al., 2012). Immediately prior to experiments, aqueous drug solution (37 ^oC;

100 □M) was prepared. Rat liver microsomal incubates were performed and included (final concentration) 2.0 mg/mL microsomal protein with NADPH (1.0 mM, cofactor for monooxygenases, *e.g.*, cytochrome P450), and (**4**; 10 □M; DMSO ≤ 0.01%, total v/v). Incubations consisted of phosphate buffer (100 mM; pH 7.4), MgCl2 (5.0 mM), and EDTA (0.1 mM). Incubations were performed as follows: (i) a mixture of phosphate buffer, MgCl2, NADPH, and microsomal protein were pre-incubated at 37.0 ± 0.1 °C for 10 min; (ii) incubations were initiated by test compound (10 □M final; 37.0 ± 0.1 °C) addition and mixing. After incubating (0.5, 5, 10, 15, 30 and 60 min) samples were removed and added to three volumes of quench solution (cold acetonitrile). The resulting samples were mixed and immediately analyzed by LC/MS-MS to probe for Phase I *in vitro* metabolism.

3.4.6 Organic Anion Transporter (OAT) in vitro studies: From transgenic mice harboring the simian virus 40 large T-antigen gene, S2-hOAT1, S2-hOAT2, S2-hOAT3, and S2-hOAT4 were established and characterized as previously reported (Enomoto et al., 2002; Hosoyamada et al., 1996; Takeda et al., 2002; Kimura et al., 2002). Briefly, the full-length cDNAs of hOATs were sub-cloned into pcDNA 3.1 (Invitrogen), a mammalian expression vector. S2-hOATs were obtained by transfecting S2 cells with the vectors that coupled with pSV2neo – a neomycin resistance gene – using TfX-50 and according to the manufacturer's instructions. S2 cells transfected with pcDNA3.1 lacking an insert and pSV2neo were designated as S2 pcDNA 3.1 (mock) and used as control. Cells were grown in a humidified incubator (33 °C) and under 5% CO2 using Dulbecco's Modified Eagle's Medium/Nutrient F-12 Ham (DMEM:Ham's F-12; 1:1) containing 5% FBS, transferrin (10 µg/mL), insulin (0.08 U/mL), recombinant epidermal growth factor (10 ng/mL), and geneticin (400 µg/mL). The cells were sub-cultured in a medium containing 0.05% trypsin-EDTA solution (containing 137 mM NaCl, 5.4 mM KCl, 5.5 mM glucose, 4.0 mM NaHCO3, 0.50 mM EDTA, and 5.0 mM HEPES; pH 7.2) and passage numbers 25-27 were used.

Uptake experiments were performed as previously described (Hosoyamada et al., 1996; Enomoto et al., 2002; Kimura et al., 2002; Takeda et al., 2002). The S2-cells were seeded into 24-well tissue culture plates at a density of 1.0×10^5 cells/well. After the cells were cultured (2 days), the cells were washed three times with Dulbecco's modified phosphate-buffered saline solution (containing 137 mM NaCl, 3.0 mM KCl, 8.0 mM NaHPO4, 1.0 mM KH2PO4, 1.0 mM CaCl2, and 0.50 mM MgCl2, pH 7.4) supplemented with 5.5 mM glucose and then pre-incubated (10 min) in the same solution in a water bath (37 °C). To evaluate the transport mediated by hOAT1, hOAT2, hOAT3, and hOAT4, S2-cells were incubated (37 °C) in the absence or presence of (**4**; 1.0 □M). Uptake experiments were stopped (1.0, 5.0 and 10.0 min) by the addition of ice-cold Dulbecco's modified phosphate-buffered saline solution, and the cells were washed three times with the same solution. The cells in each well were mixed with organic solvent extraction (1:4; water:methanol solution, 500 □L), transferred to eppendorf tubes (1.5 mL), sonicated (5.0 min), centrifuged (10,000 rpm, 5.0 min) and then samples were transferred to a 96-well plate and the drug concentrations were determined via LC/MS-MS methods.

3.4.7 LC/MS-MS methods: Liquid chromatography employed an Agilent Technologies, Zorbax extended-C18 50 x 4.6 mm (5 micron) at 40 °C with 0.4 mL/min flow rate. Mobile phase A was HPLC grad water containing 10 mM (NH4OAc) and 0.1% formic acid; while solvent B was 50:50 ACN:MeOH. The chromatography method used was as follows: 95% A (1.0 min); ramped to 95% B at 5.5 min, held (2.5 min), and returned to 95% A (9.0 min) and held (1.0 min; 10 min total run time). GSK126 **4**, deuterated IS **29**, and metabolites were observed via electro-spray ionization positive ion mode (ESI+) using the following conditions: i) ion-spray

voltage of 5500 V; ii) temperature, 450 ^{o}C; iii) curtain gas (CUR; set at 10) and Collisionally Activated Dissociation (CAD; set at 12) gas were nitrogen; iv) Ion Source gas one (GS1) and two (GS2) were set at 30; v) entrance potential was set at 10 V; vi) quadruple one (Q1) and (Q3) were set on Unit resolution; vii) dwell time was set at 200 msec; and viii) declustering potential (DP), collision energy (CE), and collision cell exit potential (CXP) are voltages (V). Samples (10 □L) were analyzed by LC/MS-MS: GSK126 **4** 527.4 □ 375.2 m/z, DP (91), CE (35), CXP (10); IS **29** 534.4 □ 375.3 *m/z*, DP = (86), CE (35), CXP (10); M + O metabolites 543.4 □ 375.2 *m/z* and 543.3 □ 391.3 *m/z* at DP (91), CE (35) and CXP (10). The supplementary materials section provides MS/MS and LC/MS-MS examples of **4** and **29**.

3.4.8 Sprague-Dawley Rat tissue distribution and Pharmacokinetic Studies: The *in vivo* experiments were conducted at East Tennessee State University – Quillen College of Medicine – in an AAALAC accredited facility. All procedures were reviewed and approved by the ETSU Committee on Animal Care; the research procedures adhered to the 'Principles of Laboratory Animal Care' (NIH publication #85-23, revised in 1985). Male SD rats were purchased from Harlan World Headquarters (Indianapolis, Indiana, USA) and upon arrival were acclimated to their new surroundings (one week) and housed in groups of three (22 ± 1 ^{o}C; 55 ± 15% humidity, 12 h dark/light cycles). Animals had free access to water, but were fasted 14 ± 2 h prior to dosing. SD rats were dosed in the morning, approximately 2-3 h after the begging of a light cycle.

Fasted animals (297 ± 15 g) were then dosed via: i) ophthalmic venous plexus (orbital sinus) using a syringe (1.0 mL disposable employing a 27G needle); ii) capsule dosing with a Torpac capsule syringe (Torpac, USA) and followed with a water (HPLC grade; 500 µL); or iii) a gavage solution/suspension. Drug and control CMC formulations were prepared by weighing the synthesized **4** into a glass vial containing CMC, four weight equivalents. A stir vane was added, capped, and stirred (1.0 h); afterwards, the mixed blend containing approximately 20 weight percent **4** was used to prepare hand-packed capsules using a filling funnel and encapsulated into hard shell Torpac Lock ring gel (size 9) capsules (Torpac, USA).

Ophthalmic venous plexus (orbital sinus dosing, OSD) doses were prepared immediately prior to dosing as aqueous solutions containing 10% DMSO. OSD dosed SD rats were anaesthetized with isoflurane and subsequently infused (300 µL over < 30 s) with corresponding drug solution via OSD. Utilizing tail-vein collection (the anterior portion was transected, 2-3 mm), blood samples (125 µL) were acquired using mini-capillary blood collection tubes containing EDTA di-potassium salt (SAFE-T-FILL®; RAM Scientific Inc., Yonkers, NY, USA). Animals receiving an OSD dose had blood samples collected at time (min) 2, 5, 10, 15, 30, 45, 60 (1.0 h), 90, 120 (2.0 h), 150, 180 (3.0 h), 210, and 240 (4.0 h) min post-dose. Animals dosed with capsules, or via gavage solution, had blood samples taken at 15, 30, 60 min (1.0 h), 90, 120 (2.0 h), 2.5 h, 3.0 h, 3.5 h, 4.0 h, 6.0 h, 8.0 h, and 24 h post-dose.

When urine (0-8 h sample time collected on ice) was collected, fed animals were dosed via OSP and housed in metabolic cages with water, *ad libitum* free access to water; food was not returned until after the 8.0 h experiment. In the case of the tissue distribution experiments, animals were euthanized (CO2) and their blood, brains, kidneys and livers were individually harvested and immediately frozen and stored frozen (-80 ± 10 □C) until sample preparation and subsequent LC/MS-MS analysis. Control SD blood (K2 EDTA) and tissues (brains, kidneys and livers) were used to prepare standard curves from the different biological matrices. Control and sample tissues were homogenized with 2.0 mL PBS (phosphate buffer saline; pH 7.4)

for every 1.0 g tissue. Standard curves (SC) were prepared by addition with thorough mixing of various aqueous drug solutions (50 □L) into control blood or homogenate (950 □L); these were diluted serially to produce SC samples and also QC (quality control) samples. These samples were immediately frozen and stored (-80 ± 10 □C), undergoing one freeze thaw cycle as per the actual samples, prior to sample preparation and LC/MS-MS analysis.

When ready to analyze, blood samples (tissues or urine samples) were removed in sets from the freezer and allowed to thaw on the bench-top (15 – 20 min) until signs of being thawed were obvious upon visual inspection, but samples were still cold. To ensure homogeneity, the blood samples were vortex mixed (5 sec), the caps opened and extraction solution (250 □L) added, re-capped, vortex mixed (5 s), sonicated in a water bath (5 min), vortex mixed (5 s) a second time, and then centrifuged (10,000 rpm; 10 min) using an Eppendorf mini-spin centrifuge (Hamburg, Germany). The extraction solution was freshly prepared by mixing water (100 mL) with methanol:acetonitrile (1:1; 300 mL); the stock DMSO internal standard **24** was then spiked into the extraction solution and mixed. The supernatants were transferred into individual wells of a 96-well plate, placed into the LEAP auto-sampler cool-stack (8.0 ± 1.0 ^{o}C) and immediately analyzed via LC/MS-MS. In the case of the tissues, homogenates were prepared as per the standard curves, on a 1.0 g to every 2.0 mL PBS ratio (w/v); complete tissues were homogenized and samples were collected in triplicates and extracted in a 1:2 sample:extraction solution format as previously described. The individual standard curves (no matrix, blood, brain, kidney and liver) were separately used to determine the apparent drug concentrations from the biological samples.

3.4.9 Software and statistics: Pharmacokinetic (PK) data were computed using non-compartmental analysis model via linear trapezoidal rule via software program WinNonlin® (Phoenix Pharsight v6.3). Analyst 1.4.2 was used for LC/MS-MS data acquisition. Prism 4.02™ (GraphPad Software, Inc.; San Diego, CA) was used to graph and perform statistical analysis. Chemical structures were prepared using ChemBioDraw Ultra 12.0 (CambridgeSoft; Cambridge, MA). The statistical differences in **Figure 2A** were compared using one-way analysis of variance followed by a Tukey's multiple comparison test; ns = P > 0.5; *** = P < 0.001. **Figures 3A**, **3B**, and **5** were compared using one-way analysis of variance followed by a Dunnett's Multiple Comparison Test at the 95% confidence level; significance denoted as; ns = P > 0.5, * = P < 0.01. The AUC and T1/2 comparisons were performed via a paired t-test.

Acknowledgments

KA, KV, and MFW conducted chemical synthesis. JWL, PJR and MFW designed and conducted *in vivo* experiments. We wish to thank Dr. Gregory A. Hanley at ETSU for his assistance to JWL regarding *in vivo* orbital sinus dosing. ALL, PJ, HE and MFW contributed in the design and execution of drug transporter studies. MN and JFP performed experiments on KO99L cells and analyzed the data. MFW performed the *in vitro* metabolism experiments. The research utilized services of the Medicinal Chemistry Core Facility (MCCF) housed within the Department of Pharmaceutical Sciences (DOPS). RV and PR commissioned the MCCF to prepare compound **4** for their research interests; work supported by the Department of Pediatrics, University of Colorado Anschutz medical campus. The MCCF receives funding via CCTSI, an institute at the University of Colorado Denver supported in part by NIH/NCATS

Colorado CTSI Grant Number UL1TR001082.

References

Alimova, I.; Venkataraman, S.; Harris, P.; Marquez, V. E.; Northcott, P. A.; Dubuc, A.; Taylor, M. D.; Foreman, N. K.; Vibhakar, R. 2012. Targeting the enhancer of zeste homologue 2 in medulloblastoma. Int J Cancer, 131:1800-1809.

Alimova, I.; Birks, D. K.; Harris, P. S.; Knipstein, J. A.; Venkataraman, S.; Marquez, V. E.; Foreman, N. K.; Vibhakar, R. 2013. Inhibition of EZH2 suppresses self-renewal and induces radiation sensitivity in atypical rhabdoid teratoid tumor cells. Neuro Oncol, 15:149-60.

Anzai, N.; Wakui, S.; Jutabha, P.; Muto, T.; Hayashi, M.; Hayashi, K.; Domae, M.; Uchida, K.; Wempe, M. F.; Endou, H. 2011. Human Drug Transporter Gene-expressing Cells are Useful Alternatives to Predict Pharmacokinetics in Man. AATEX, 16:66-73.

Be´guelin, W.; Popovic, R.; Teater, M.; Jiang, Y.; Bunting, K. L.; Rosen, M.; Shen, H.; Yang, S. N.; Wang, L.; Ezponda, T.; Martinez-Garcia, E.; Zhang, H.; Zheng, Y.; Verma, S. K.; McCabe, M. T.; Ott, H. M.; Van Aller, G. S.; Kruger, R. G.; Liu, Y.; McHugh, C. F.; Scott, D. W.; Chung, Y. R.; Kelleher, N.; Shaknovich, R.; Creasy, C. L.; Gascoyne, R. D.; Wong, K-K.; Cerchietti, L.; Levine, R. L.; Abdel-Wahab, O.; Licht, J. D.; Elemento, O.; Melnick, A. M. 2013. EZH2 is required for germinal center formation and somatic EZH2 mutations promote lymphoid transformation. Cancer Cell, 23:677–692.

Bhasin, M.; Reinherz, E. L.; Reche, P. A. 2006. Recognition and classification of histones using support vector machine. Journal of Computational Biology, 13:102-112.

Brackley, J.; Burgess, J.L.; Grant, S.; Johnson, N.; Knight, S.D.; LaFrance, L.; Miller, W.H.; Newlander, K.; Romeril, S.; Rouse, M.B.; Tian, X.; Verma, S.K. 2011. International Application Published Under the Patent Cooperation Treaty (PCT). WO 2011/140324 A1.

Cardoso, C.; Mignon, C.; Hetet, G.; Grandchamps, B.; Fontes, M.; Colleaux, L. 2000. The human EZH2 gene: genomic organisation and revised mapping in 7q35 within the critical region for malignant myeloid disorders. European Journal of Human Genetics, 8:174–180.

Chiba, S.; Ikawa, T.; Takeshita, H.; Kanno, S.; Nagai, T.; Takada, M.; Mukai, T.; Wempe, M. F. 2013. Human organic cation transporter 2 (hOCT2): Inhibitor studies using S2-hOCT2 cells. Toxicology, 310:98-103.

Crea, F.; Hurt, E. M.; Mathews, L. A.; Cabarcas, S. M.; Sun, L.; Marquez, V. E.; Danesi, R.; Farrar, W. L. 2011. Pharmacologic disruption of Polycomb Repressive Complex 2 inhibits tumorigenicity and tumor progression in prostate cancer. Molecular Cancer, 10:40.

Enomoto, A.; Takeda, M.; Shimoda, M.; Narikawa, S.; Kobayashi, Y.; Kobayashi, Y.; Yamamoto, T.; Sekine, T.; Cha, S. H.; Niwa, T.; Endou, H. 2002. Interaction of human organic anion transporters 2 and 4 with organic anion transport inhibitors. J Pharmacol Exp Ther, 301:797-802.

Hagenbeek, T. J.; Naspetti, M.; Malergue, F.; Garcon, F.; Nunes, J. A.; Cleutjens, K. B.; Trapman, J.; Krimpenfort, P.; Spits, H. 2004. The loss of PTEN allows TCR alphabeta lineage thymocytes to bypass IL-7 and Pre-TCR-mediated signaling. J Exp Med, 200:883-894.

Harris, P. S.; Venkataraman, S.; Alimova, I.; Birks, D. K.; Donson, A. M.; Knipstein, J.; Dubuc, A.; Taylor, M. D.; Handler, M. H.; Foreman, N. K.; Vibhakar, R. 2012. Polo-like kinase 1 (PLK1) inhibition suppresses cell growth and enhances radiation sensitivity in medulloblastoma cells. BMC Cancer, 12:80, 1471-2407-12-80.

Hosoyamada, M.; Obinata, M.; Suzuki, M.; Endou, H. 1996. Cisplatin-induced toxicity in immortalized renal cell lines established from transgenic mice harboring temperature sensitive SV40 large T-antigen gene. Arch Toxicol., 70:284-292.

Kimura, H.; Takeda, M.; Narikawa, S.; Enomoto, A.; Ichida, K.; Endou, H. 2002. Human organic anion transporters and human organic cation transporters mediate renal transport of prostaglandins. J Pharmacol Exp Ther., 301:293-298.

Kleer, C. G.; Cao, Q.; Varambally, S.; Shen, R.; Ota, I.; Tomlins, S. A.; Ghosh, D.; Sewalt, R. G.; Otte, A. P.; Hayes, D. F.; Sabel, M. S.; Livant, D.; Weiss, S. J.; Rubin, M. A.; Chinnaiyan, A. M. 2003. EZH2 is a marker of aggressive breast cancer and promotes neoplastic transformation of breast epithelial cells. Proc. Natl Acad. Sci., 100:11606–11611.

Kleer, C.G. 2009. Carcinoma of the breast with medullary-like features: diagnostic challenges and relationship with BRCA1 and EZH2 functions. Arch Pathol Lab Med., 133:1822-1825.

Knutson, S. K.; Wigle, T. J.; Warholic, N. M.; Sneeringer, C. J.; Allain, C. J.; Klaus, C. R.; DSacks, J.; Raimondi, A.; Majer, C. R.; Song, J.; Scott, M. P.; Jin, L.; Smith, J. J.; Olhava, E. J.; Chesworth, R.; Moyer, M. P.; Richon, C. M.; Copeland, R. A.; Keilhack, H.; Pollock, R. M.; Kuntz, K. W. 2012. A selective inhibitor of EZH2 blocks H3K27 methylation and kills mutant lymphoma cells. Nature chemical Biology, 8:890-896.

Konze, K. D.; Ma, A.; Li, F.; Barsyte-Lovejoy, D.; Parton, T.; MacNevin, C. J.; Liu, F.; Gao, C.; Huang, X-P.; Kuznetsova, E.; Rougie, M.; Jiang, A.; Pattenden, S. G.; Norris, J. L.; James, L. I.; Roth, B. L.; Brown, P. J.; Frye, S. V.; Arrowsmith, C. H.; Hahn, K. M.; Wang, G. G.; Vedadi, M.; Jin, J. 2013. An orally bioavailable chemical probe of the Lysine Methyltransferases EZH2 and EZH1. ACS Chem. Biol., 8:1324−1334.

McCabe, M. T.; Ott, H. M.; Ganji, G.; Korenchuk, S.; Thompson, C.; Van Aller, G. S.; Liu, Y.; Graves, A. P.; Pietra III, A. D.; Diaz, E.; LaFrance, L. V.; Mellinger, M.; Duquenne, C.; Tian, X.; Kruger, R. G.; McHugh, C. F.; Brandt, M.; Miller, W. H.; Dhanak, D.; Verma, S. K.; Tummino, P. J.; Creasy, C. L. 2012. EZH2 inhibition as a therapeutic strategy for lymphoma with EZH2-activating mutations. Nature, 492:108-112.

Miranda, T. B.; Cortez, C. C.; Yoo, C. B.; Liang, G.; Abe, M.; Kelly, T. K.; Marquez, V. E.; Jones, P. A. 2009. DZNep is a global histone methylation inhibitor that reactivates developmental genes not silenced by DNA methylation. Mol Cancer Ther, 8:1579-1588.

Pritchard, J. B.; Miller, D. S. 1993. Mechanisms mediating renal secretion of organic anions and cations. Physiol Rev, 73:765-796.

Qi, W.; Chana, H.; Teng, L.; Li, L.; Chuai, S.; Zhang, R.; Zeng, J.; Li, M.; Fan, H.; Lin, Y.; Gu, J.; Ardayfio, O.; Zhang, J-H.; Yan, X.; Fang, J.; Mi, Y.; Zhang, M.; Zhou, T.; Feng, G.; Chen, Z.; Li, G.; Yang, T.; Zhao, K.; Liu, X.; Yu, Z.; Lu, C.X.; Atadja, P.; Li, E. 2012. Selective inhibition of Ezh2 by a small molecule inhibitor blocks tumor cells proliferation**.** Pro. Nat. Acc. Sci., 109:21360-21365.

Rosilio, C.; Nebout. M.; Imbert. V.; Griessinger, E.; Neffati, Z.; Benadiba, J.; Hagenbeek, T.; Spits, H.; Reverso, J.;

Ambrosetti, D.; Michiels, J. F.; Bailly-Maitre, B.; Endou, H.; Wempe, M. F. Peyron, J. F. 2015. L-type amino-acid transporter 1 (LAT1): a therapeutic target supporting growth and survival of T-cell lymphoblastic lymphoma/T-cell acute lymphoblastic leukemia. Leukemia, in press. Dec 8. doi: 10.1038/leu.2014.338. [Epub ahead of print] PMID: 25482130.

Smits, M.; Nilsson, J.; Mir, S. E.; Van der Stoop, P. M.; Hulleman, E.; Niers, J. M.; de Witt Hamer, P. C.; Marquez, V. E.; Cloos, J.; Krichevsky, A. M.; Noske, D. P., Tannous, B. A.; Würdinger, T. 2010. miR-101 is down-regulated in glioblastoma resulting in EZH2-induced proliferation, migration, and angiogenesis. Oncotarget, 1:710 – 720.

Takawa, M.; Masuda, K.; Kunizaki, M.; Daigo, Y.; Takagi, K.; Iwai, Y.; Cho, H. S.; Toyokawa, G.; Yamane, Y.; Maejima, K.; Field, H. I.; Kobayashi, T.; Akasu, T.; Sugiyama, M.; Tsuchiya, E.; Atomi, Y.; Ponder, B. A.; Nakamura, Y.; Hamamoto, R. 2011. Validation of the histone methyltransferase EZH2 as a therapeutic target for various types of human cancer and as a prognostic marker. Cancer Sci., 102:1298-1305.

Takeda, M.; Khamdang, S.; Narikawa, S.; Kimura, H.; Kobayashi, Y.; Yamamoto, T.; Cha, S. H.; Sekine, T.; Endou, H. 2002. Human organic anion transporters and human organic cation transporters mediate renal antiviral transport. J Pharmacol Exp Ther, 300:918-924.

Tan, J.; Yang, X.; Zhuang, L.; Jiang, X.; Chen, W.; Lee, P. L.; Karuturi, R. K.; Tan, P. B.; Liu, E. T.; Yu, Q. 2007. Pharmacologic disruption of Polycomb-repressive complex 2-mediated gene repression selectively induces apoptosis in cancer cells. Genes Dev, 21:1050–1063.

Varambally, S.; Dhanasekaran, S. M.; Zhou, M.; Barrette, T. R., Kumar-Sinha, C.; Sanda, M. G.; Ghosh, D.; Pienta, K. J.; Sewalt, R. G.; Otte, A. P.; Rubin, M. A.; Chinnaiyan, A. M. 2002. The polycomb group protein EZH2 is involved in progression of prostate cancer. Nature, 419:624-629.

Varambally, S.; Cao, Q.; Mani, R. S.; Shankar, S.; Wang, X.; Ateeq, B.; Laxman, B.; Cao, X.; Jing, X.; Ramnarayanan, K.; Brenner, J. C.; Yu, J.; Kim, J. H.; Han, B.; Tan, P.; Kumar-Sinha, C.; Lonigro, R. J.; Palanisamy, N.; Maher, C. A.; Chinnaiyan, A. M. 2008. Genomic loss of microRNA-101 leads to overexpression of histone methyltransferase EZH2 in cancer. Science, 322:1695-1699.

Verma, S. K.; Tian, X.; LaFrance, L. V.; Duquenne, C.; Suarez, D. P.; Newlander, K. A.; Romeril, S. P.; Burgess, J. L.; Grant, S. W.; Brackley, J. A.; Graves, A. P.; Scherzer, D. A.; Shu, A.; Thompson, C.; Ott, H. M.; Van Aller, G. S.; Machutta, C. A.; Diaz, E.; Jiang, Y.; Johnson, N. W.; Knight, S. D.; Kruger, R. G.; McCabe, M. T.; Dhanak, D.; Tummino, P. J.; Creasy, C. L.; Miller, W. H. 2012. Identification of Potent, Selective, Cell-Active Inhibitors of the Histone Lysine Methyltransferase EZH2. Med. Chem. Lett., 3:1091−1096.

Wagener, N.; Holland, D.; Bulkescher, J.; Crnković-Mertens, I.; Hoppe-Seyler, K.; Zentgraf, H.; Pritsch, M.; Buse, S.; Pfitzenmaier, J.; Haferkamp, A.; Hohenfellner, M.; Hoppe-Seyler, F. 2008. The enhancer of zeste homolog 2 gene contributes to cell proliferation and apoptosis resistance in renal cell carcinoma cells. Int. J. Cancer, 123:1545-1550.

Wagener, N.; Macher-Goeppinger, S.; Pritsch, M.; Hüsing, J.; Hoppe-Seyler, K.; Schirmacher, P.; Pfitzenmaier, J.; Haferkamp, A.; Hoppe-Seyler, F.; Hohenfellner, M. 2010. Enhancer of zeste homolog 2 (EZH2) expression is an independent prognostic factor in renal cell carcinoma. BMC Cancer, 10:524.

Warburg, O. 1956. On the origin of cancer cells. Science, 123:309-314.

Wempe, M. F.; Lightner, J. W.; Miller, B.; Iwen, T. J.; Rice, P. J.; Wakui, A.; Anzai, N.; Jutabha, P.; Endou, H. 2012. Potent human uric acid transporter 1 inhibitors: in vitro and in vivo metabolism and pharmacokinetic studies. Drug Design, Development and Therapy, 6:323-339.

Yan, J.; Ng, S-B.; Tay, J. L-S.; Lin, B.; Koh, T.L.; Tan, J.; Selvarajan, V.; Liu, S-C; Bi, C.; Wang, S.; Choo, S-N.; Shimizu, N.; Huang, G.; Yu, Q.; Chng W-J. 2013. EZH2 overexpression in natural killer/T-cell lymphoma confers growth advantage independently of histone methyltransferase activity. Blood, 121:4512-4520.

Yanagida, O.; Kanai, Y.; Chairoungdua, A.; Kim, D. K.; Segawa, H.; Nii, T.; Cha, S. H.; Matsuo, H.; Fukushima, J.; Fukasawa, Y.; Tani, Y.; Taketani, Y.; Uchino, H.; Kim, J. Y.; Inatomi, J.; Okayasu, I.; Miyamoto, K.; Takeda, E.; Goya, T.; Endou, H. 2001. Human L-type amino acid transporter 1 (LAT1): characterization of function and expression in tumor cell lines. Biochim Biophys Acta, 2:291-302.

Zeidler, M.; Kleer, C. G. 2006. The Polycomb group protein Enhancer of Zeste 2: its links to DNA repair and breast cancer. J Mol Hist., 37:219–223.

Supplementary Material Section

EZH2 INHIBITOR GSK126 FOR CANCER TREATMENT: METABOLISM, DRUG TRANSPORTER AND RAT PHARMACOKINETIC STUDIES

Amit Kumar[a]; Vijay Kumar[a]; Janet W. Lightner[b]; Anaheed L. Little[a]; Promsuk Jutabha[c]; Hitoshi Endou[d]; Peter J. Rice[a,b]; Philip Reigan[a]; Rajeev Vibhakar[e]; Peter Harris[e]; Ilango Balakrishnan[e]; Sujatha Venkataraman[e]; Marielle Nebout[f]; Jean-Francois Peyron[f]; and Michael F. Wempe[a,g,]*

* Corresponding Author: Michael F. Wempe Michael F. Wempe, PhD
michael.wempe@ucdenver.edu
(T) 303-724-8982
(F) 303-724-6148

[a]Department of Pharmaceutical Sciences, School of Pharmacy, University of Colorado Denver Anschutz Medical Campus, Aurora, CO 80045, USA
[b]Department of Pharmacology, East Tennessee State University Johnson City, TN 37614, USA
[c] Dokkyo Medical University School of Medicine, Tochigi, Japan
[d]Department of Pharmacology and Toxicology, Kyorin University School of Medicine, Mitaka, Tokyo, 181-8611 Japan
[e] Department of Pediatrics, School of Medicine, University of Colorado Denver, Anschutz Medical Campus, Aurora, CO 80045, USA
[f]INSERM, U1065, Centre Méditerranéen de Médecine Moléculaire (C3M), Equipe Inflammation, Cancer, Cellules Souches Cancéreuses, Nice, France.
[g]University of Colorado Cancer Center, University of Colorado Denver, Aurora, Colorado 80045, USA

∗ Corresponding author. Tel.: 303-724-8982; fax: 303-724-6148; e-mail: michael.wempe@ucdenver.ed

S-Figure 1 MS-MS of deuterated GSK126

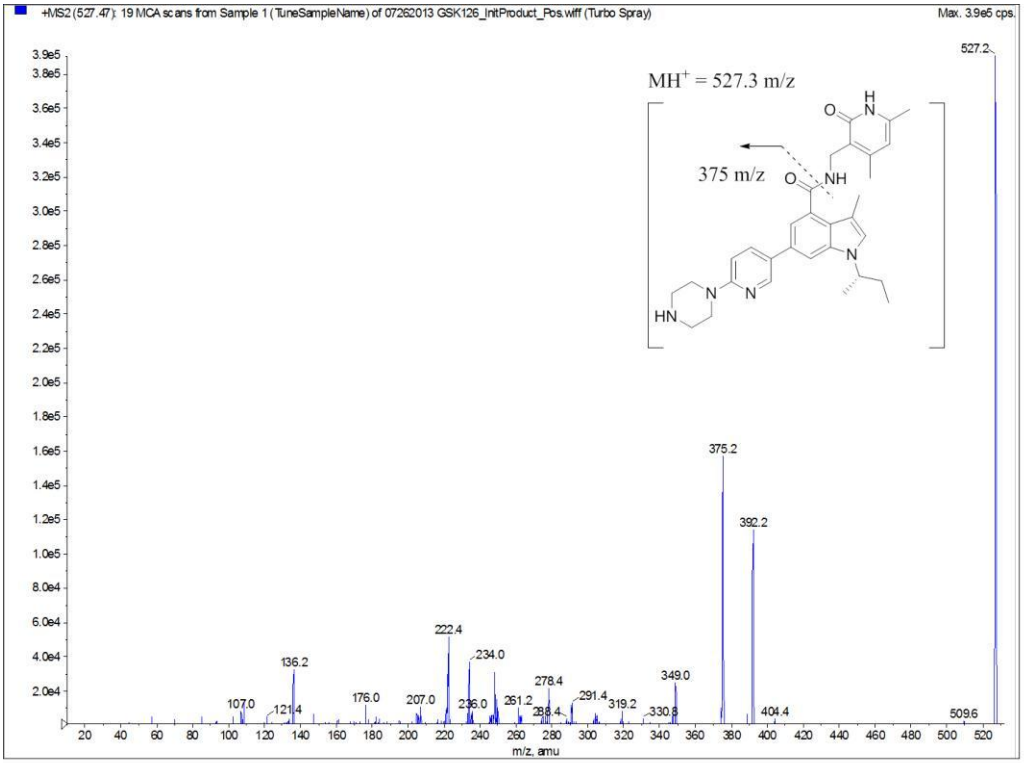

S-Figure 2 MS-MS of deuterated GSK126-d7

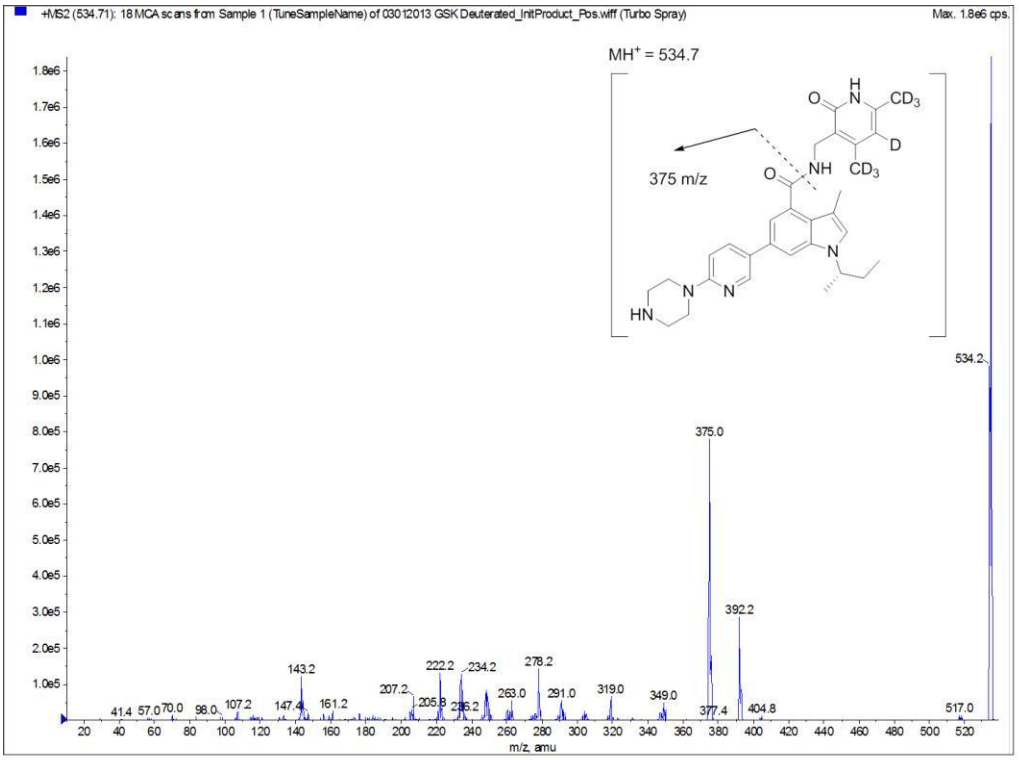

S-Figure 3 LC/MS-MS example of GSK126-d7

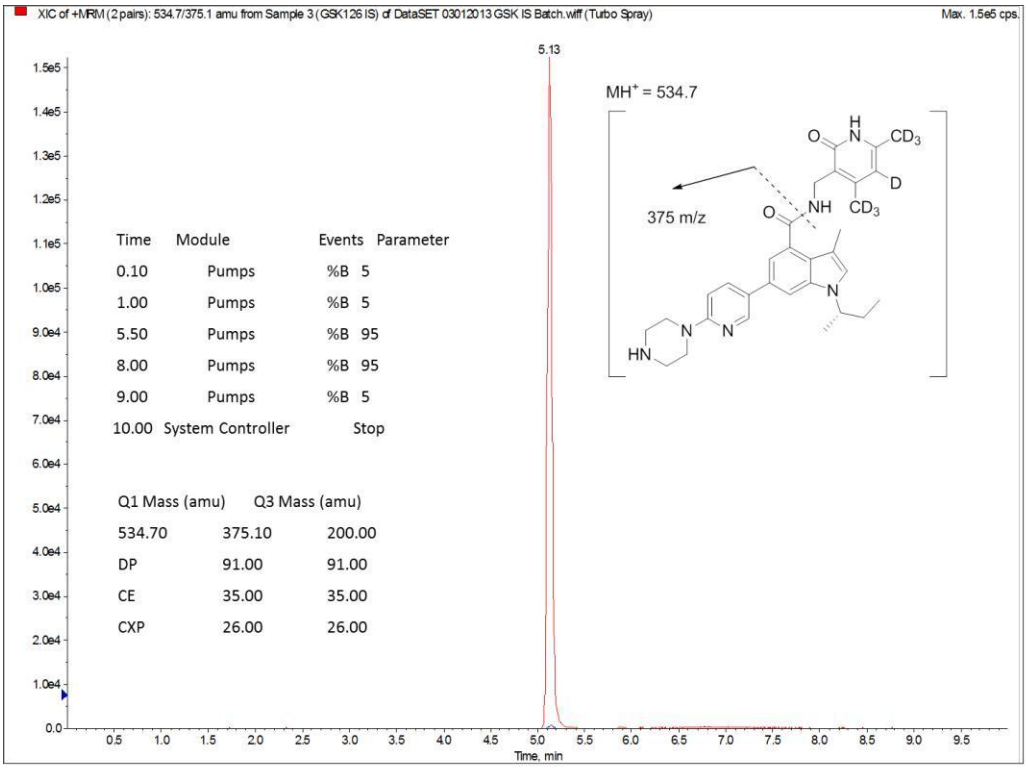

S-Figure 4 LC/MS-MS example of GSK126 and GSK126-d7